frontiers | Frontiers in Earth Science

TYPE Original Research
PUBLISHED 24 January 2023
DOI 10.3389/feart.2022.1070004

OPEN ACCESS

EDITED BY
Zhigang Li,
Sun Yat-sen University, China

REVIEWED BY
Xiwu Luan,
Qingdao National Laboratory for Marine Science and Technology, China
Junling Pei,
Chinese Academy of Geological Sciences (CAGS), China

*CORRESPONDENCE
Guangzeng Wang,
wangguangzeng@ouc.edu.cn
Yanhui Suo,
suoyh@ouc.edu.cn

SPECIALTY SECTION
This article was submitted to Structural Geology and Tectonics, a section of the journal Frontiers in Earth Science

RECEIVED 14 October 2022
ACCEPTED 29 November 2022
PUBLISHED 24 January 2023

CITATION
Zhan H, Wang G, Peng G, Suo Y, Wang P, Du X, Zhou J, Li S and Zhu D (2023), Cenozoic evolution of the Yangjiang-Yitong'ansha fault zone in the northern South China Sea: Evidence from 3D seismic data.
Front. Earth Sci. 10:1070004.
doi: 10.3389/feart.2022.1070004

Cenozoic evolution of the Yangjiang-Yitong'ansha fault zone in the northern South China Sea: Evidence from 3D seismic data

Huawang Zhan[1,2], Guangzeng Wang[1,2]*, Guangrong Peng[3], Yanhui Suo[1,2]*, Pengcheng Wang[1,2], Xiaodong Du[3], Jie Zhou[1,2], Sanzhong Li[1,2] and Dingwei Zhu[3]

[1]Frontiers Science Center for Deep Ocean Multispheres and Earth System, Key Lab of Submarine Geosciences and Prospecting Techniques, MOE and College of Marine Geosciences, Ocean University of China, Qingdao, China, [2]Laboratory for Marine Mineral Resources, Qingdao National Laboratory for Marine Science and Technology, Qingdao, China, [3]Shenzhen Branch, CNOOC China Limited, Shenzhen, Guangdong, China

The Yanjiang-Yitong'ansha Fault Zone (YYFZ) traverses the Pearl River Mouth Basin (PRMB) and plays an essential role in basin formation and hydrocarbon accumulation in the PRMB. Because of the lack of seismic data, its distribution, evolution, and effect on the basin evolution in the Cenozoic are poorly known. Based on a detailed interpretation of 3D multi-channel seismic data and previous research results, the YYFZ was identified and characterized. It comprises a series of NW-trending strike-slip faults that exhibit horsetail and en echelon structures in the map view and flower-like or Y-shaped structures in the profile view. By comprehensively analyzing the Paleogene migration of depocenters, activity characteristics of the YYFZ-related faults, and the relationships between faults and sedimentary sequences along the YYFZ, we propose the sinistral motion of the YYFZ initiated at about 35 Ma. The YYFZ served as a transfer zone during the intense rifting in the PRMB from 65 to 35 Ma. Then due to the combined effect of the Indian-Eurasian collision to the west, the Pacific subduction to the east, and the proto-SCS slab-pull to the south, it became a sinistral transtensional fault from 35 Ma to 16.5 Ma. Our results highlight the significant role of the NW-trending fault systems in the basin formation and the regional tectonic evolution of the PRMB.

KEYWORDS

sinistral motion, dynamic mechanism, Yangjiang-Yitong'ansha fault zone, Pearl River Mouth Basin, Cenozoic evolution

1 Introduction

As one of the largest marginal basins in the western Pacific region, the South China Sea (SCS) has been studied not only for its rich hydrocarbon and mineral resources but also for its unique tectonic location that makes it an ideal natural laboratory for studying and testing modes of lithospheric extension and breakup (Sun et al., 2016; Ye et al., 2020). The Pearl River Mouth Basin (PRMB) on the northern SCS is a Cenozoic sedimentary basin undergoing multiple extension episodes during the late Cretaceous to Oligocene. Faults in the PRMB, especially the strike-slip ones, significantly impact basin formation and hydrocarbon accumulation (Hou et al., 2008; Cao et al., 2014). Previous studies indicated that many regional strike-slip fault zones develop in the PRMB and control its tectonic configuration (Figure 1; Li et al., 2012; Cheng et al., 2012; Wang et al., 2014; Wang W et al., 2017; Wang et al., 2020; Wang et al., 2021; Wang et al., 2022; Mu et al., 2022; Zhou et al., 2022). However, its formation mechanisms remain controversial. Some authors referred to the PRMB as a transtensional basin triggered by widely distributed NE-trending strike-slip faults (Xu and Zhang, 2000; Cheng et al., 2012; Li et al., 2012; Xu et al., 2014; Wang P et al., 2017; Mu et al., 2022; Zhou et al., 2022), whereas others proposed that the basin as a rift basin (Ho-Shing, 1990; Ge et al., 2020; Fu et al., 2021; Hao et al., 2021).

In the past few decades, the structural characterization of the PRMB has been one of the most studied targets (e.g., Shi et al., 2020; Huang et al., 2018; Zhang et al., 2021; Ye et al., 2020; Zhao et al., 2020; Hui et al., 2022; Ge et al., 2022). However, most of the studies mainly focus on the NE/NEE-trending faults since they control the basin's overall architecture (e.g., Liu et al., 2018; Ye et al., 2018, 2020; Zhao Y et al., 2018; Zhou et al., 2018; He et al., 2019; Zhou et al., 2019; Zhou et al., 2019; Ma B et al., 2020; Camanni and Ye, 2022; Suo et al., 2022). Less attention has been devoted to understanding the NW-trending ones, for example, the Yangjiang-Yitong'ansha Fault Zone (YYFZ). Previous studies indicate that the YYFZ is an important NW-trending strike-slip fault zone influencing crustal structure, continent-ocean transition zone, basement lithology, sedimentary facies, Mesozoic tectonic environment, Cenozoic fault strike, and basin structure in the northern

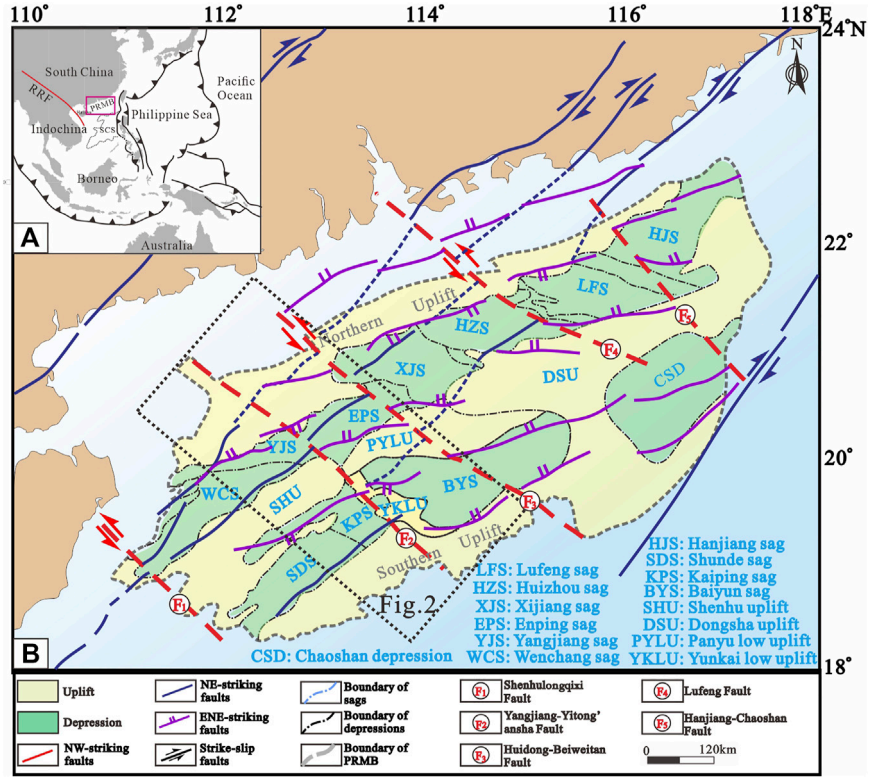

FIGURE 1
(A) Regional tectonic locations. **(B)** Structural units of the PRMB and the locations of regional strike-slip fault zone (modified after Zhu W et al., 2009; Zhu et al., 2021; Wang et al., 2020).

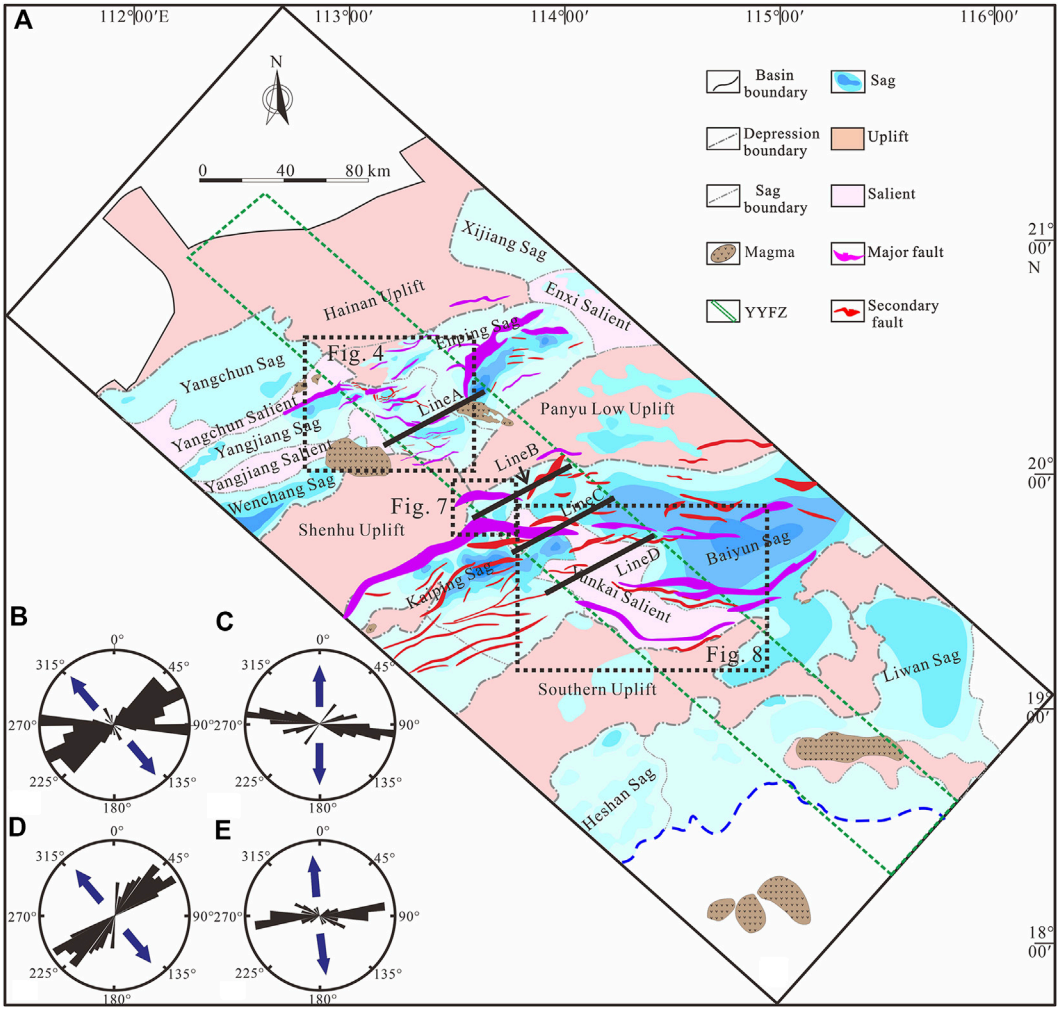

FIGURE 2
(A) Tectonic framework of the study area and the location of the YYFZ. **(B–E)** are the strike rose diagrams of major faults in the Yangjiang, Enping, Kaiping, and Baiyun sags, respectively.

SCS (Figure 2; Hu et al., 2009; Wang et al., 2006; Guo et al., 2016; Wei et al., 2011; Sun et al., 2008; Zhong et al., 2014; Liu et al., 2013; Cai et al., 2021; Sun et al., 2014; Zhu et al., 2017; Lu et al., 2011; Li et al., 2019). Owing to its specific geographical location, the YYFZ is an ideal site for investigating the NW-trending strike-slip fault zones.

The YYFZ, not often legible in shallow levels along its strike, has a complex geological history, and its origin and evolution likely had profound consequences on the formation of the PRMB (Mu et al., 2022; Wang et al., 2022). Previous research has shown that the YYFZ offset both basement gravity and magnetic anomaly belts and NE-trending faults in the PRMB and experienced marked sinistral motion during the Mesozoic (Zhou et al., 2006; Chen et al., 2005). However, limited by the low resolution of seismic data, its structural characteristics are still unclear, and its tectonic evolution remains controversial. Some authors believed that the YYFZ only exhibits a tectonic transition zone in the Cenozoic (Zhong et al., 2014; Ma M et al., 2020). Some authors considered that it experienced sinistral movements throughout the Mesozoic (Zhou et al., 2006; Chen et al., 2005; Sun et al., 2009) and was subsequently reactivated as a dextral strike-slip fault during the Cenozoic (Chen et al., 2005; Lv et al., 2017). Besides, the YYFZ is generally considered as a major sinistral strike-slip fault since the Early Oligocene (Wang et al., 2013; Sun et al., 2014; Zhang et al., 2019; Cai et al., 2021; Liu X et al., 2021; Zhan et al., 2021; Zhang et al., 2021). Further, Li et al. (2019) have confirmed the YYFZ experienced sinistral transtensional deformation in the early Cenozoic, followed by dextral transtensional deformation from about 23.8 Ma to the present, based on the comparison of structural style and tectonic evolution history on both sides of the YYFZ. However, the following essential problems about the YYFZ had not been

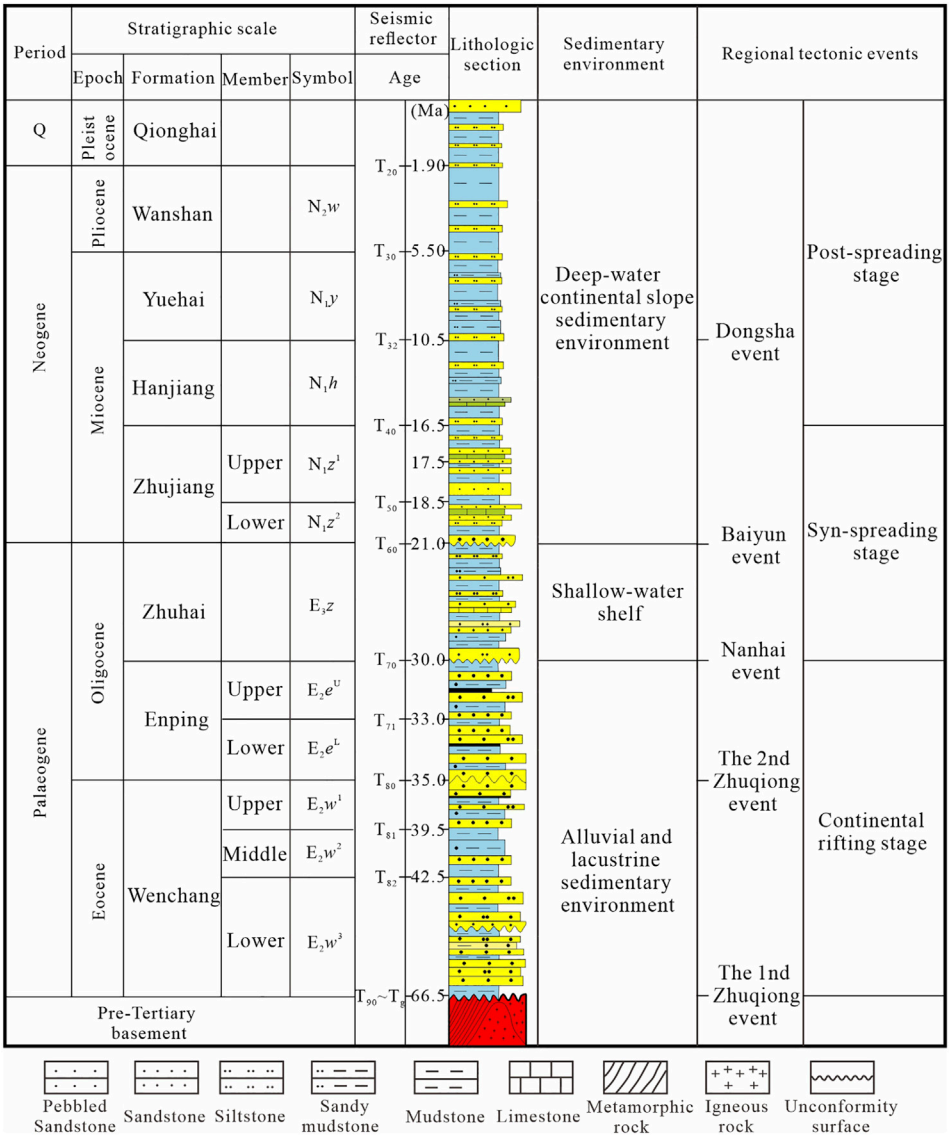

FIGURE 3
Comprehensive stratigraphic column of the PRMB showing major tectonic and depositional events (modified after Li H et al., 2014; Zhu W et al., 2009; Zhu et al., 2021; Zhang et al., 2021).

discussed clearly: 1) the structural features and initial activity of sinistral strike-slip faults, 2) the evolution history, 3) the control and influence of strike-slip fault on the evolution of the PRMB, and the driving mechanism in the Cenozoic.

In this study, we applied high-resolution 3D seismic data covering the western PRMB to investigate the YYFZ geometrical characteristics and discuss its Cenozoic evolution history. We also built a geodynamic model to reveal the influence of strike-slip fault on the evolution of the PRMB with some synchronous plate motions around the SCS in the Cenozoic. Our research has implications for understanding the complexity and diversity of faults in the PRMB and the geological evolution of the basins, which would benefit petroleum exploration there.

2 Geological setting

The PRMB, with a total area of 175,000 km^2, is a long and wide ENE-trending graben located in the northern margin of SCS. Controlled by two groups of faults with NE and NW strikes, the basin presents a segmental and zonal structural framework in the NE and NW directions, respectively (Figure 1; Cheng et al., 2012; Zhong et al., 2014). From north to south, the basin can be

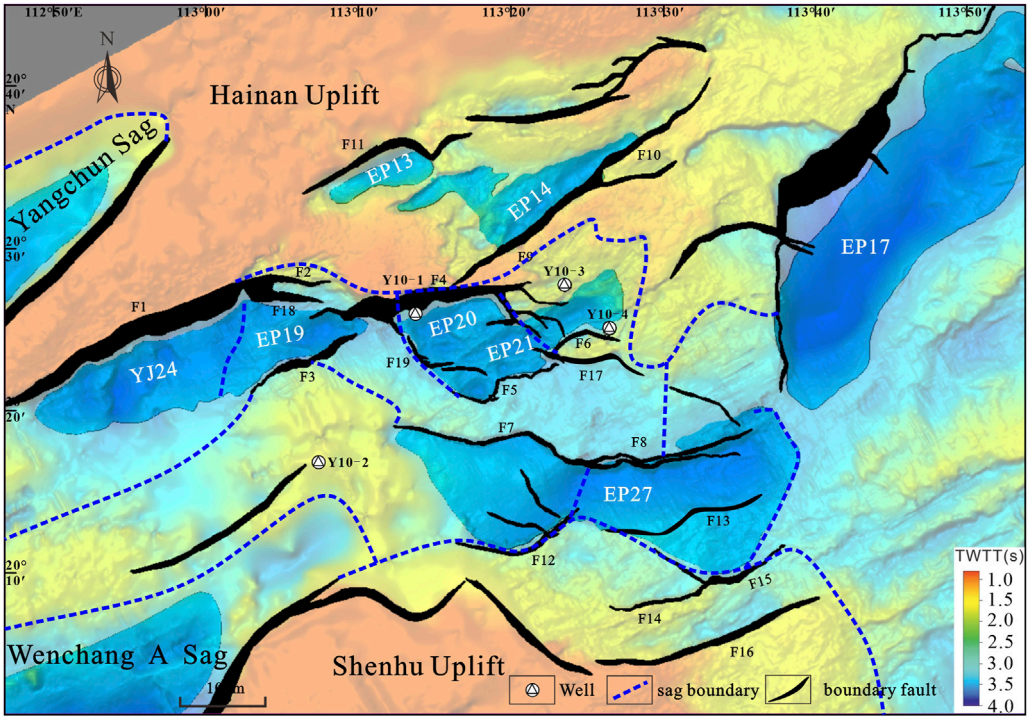

FIGURE 4
Secondary tectonic units of the Yangjiang Sag and adjacent areas (See Figure 2 for the location).

divided into five first-order structural units: the northern uplift zone, the northern depression zone, the central uplift zone, the southern depression zone, and the southern uplift zone (Xie et al., 2014; Wang P et al., 2017). The northern depression belt consists of the Zhu Ⅰ Depression (Enping Sag, Xijiang Sag, Huizhou Sag, Lufeng Sag, and Hanjiang Sag) and the Zhu Ⅲ Depression (Wenchang Sag, Yangchun Sag, Yangjiang Sag, Qionghai Sag, and Yangjiang low Uplift). The central uplift belt consists of Shenhu Uplift, Panyu low Uplift, and Dongsha Uplift from west to east. The central depression zone consists of the Zhu II Depression (Shunde Sag, Kaiping Sag, Yunkai low Uplift, and Baiyun Sag) and Chaoshan Depression. The Sag and Uplift in PRMB are mainly NE/ENE-trending. The faults developed in the PRMB during Cenozoic are mainly composed of NE-to EW-trending normal faults and NW-trending shear faults. The basin is divided into segments from west to east by NW-trending Qionghai, Yangjiang-Yitong, Huizhou, Huidong-Beiweitan, Raoping-Taixinan, Nanao-Taiwanxi faults (Chen et al., 2005).

The general stratigraphic column of the PRMB is shown in Figure 3. The Paleogene to Lower Oligocene strata consist of fluvial-lacustrine sediments in discrete rifts, among which the Eocene Wenchang and Enping Formations contain dark lacustrine mudstones that are primary source rocks for hydrocarbons in this area. Deposits in the Upper Oligocene Zhuhai Formation are transitional (alternatively coastal and littoral) and contain both source rocks and reservoirs. Neogene strata consist of marine sediments that constitute a generally transgressional sequence. The Cenozoic strata comprised seven lithostratigraphic units (Figure 3). They are from the bottom to the top, the Shenhu (E_1s) Formation, the Wenchang (E_2w) Formation, the Enping (E_2e) Formation, Zhuhai (E_3z) Formation in the Paleogene and Zhujiang (N_1z) Formation, Hanjiang (N_2h) Formation, Yuehai (N_2y) Formation and Wanshan (N_2w) Formation in the Neogene. Nine high-amplitude seismic interfaces were recognized and tracked throughout the study area: the T_{30}, T_{32}, T_{40}, T_{60}, T_{70}, T_{80}, T_{90}, and T_g. These seismic interfaces correspond to lithostratigraphic interfaces standing for the second- and third-order sequence boundaries (Ye et al., 2018).

The NEE-trending Yangjiang Sag is bounded by the Yangchun Low Uplift to the north, the Shenhu Uplift to the south, the Wenchang Sag to the west, and the Enping Sag of Zhu I depression to the east (Figure 4). Separated by the Yangjiang Low Uplift, it can be divided into the west and east sag. The structure of the west sag is north-faulted and south-overlapped, while that of the east sag is relatively complex, represented by single half-grabens and composite half-grabens. From west to east, Yangjiang Sag is further subdivided into six subsags: the YJ

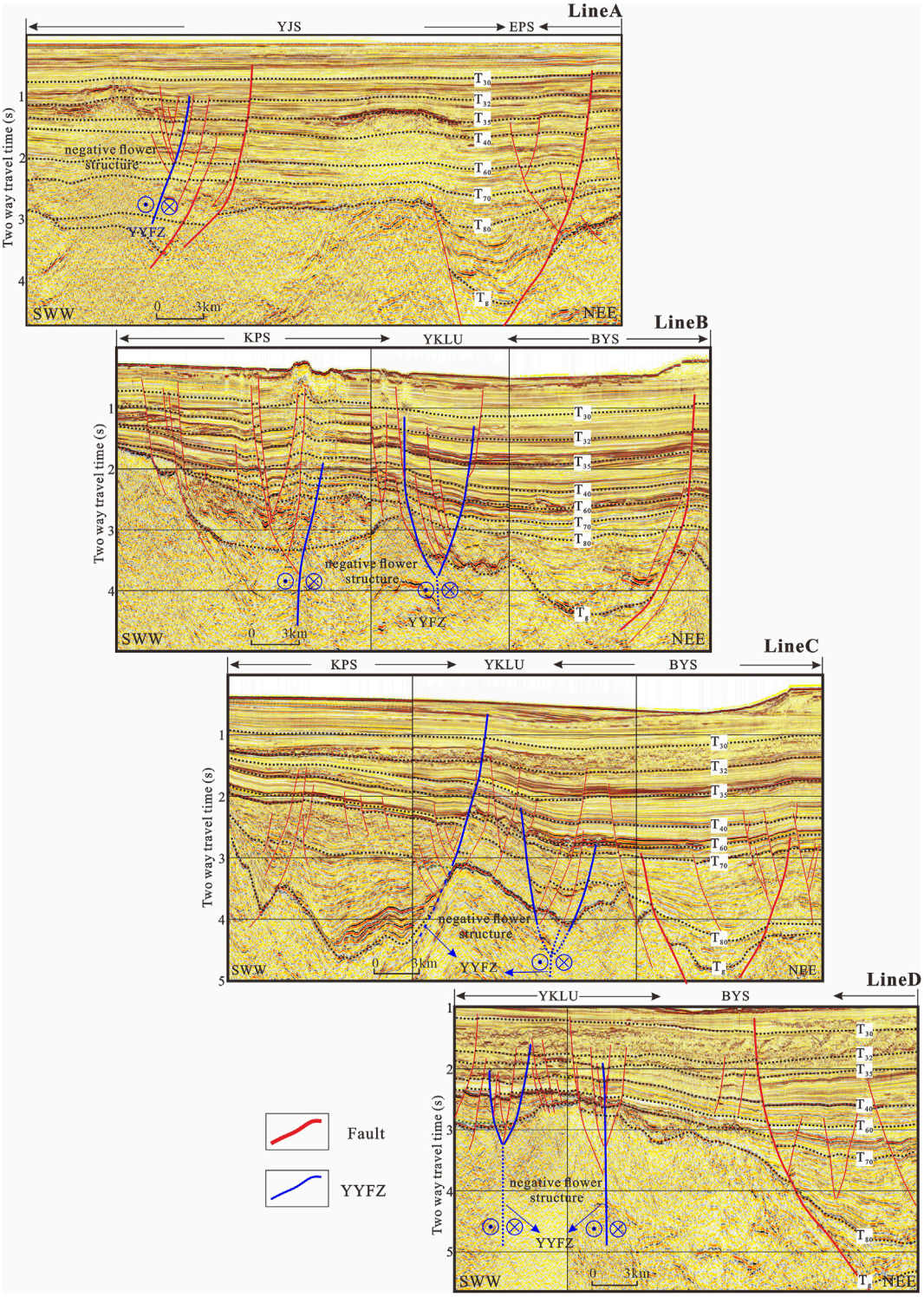

FIGURE 5
Structure, fault system, and stratum characteristics of the YYFZ. Profile locations are shown in Figure 2. The faults derived from the YYFZ terminate mainly in N_2w.

33, YJ 24, EP19, EP20, EP21, and EP27 subsags. The YJ33 and YJ24 subsags are bounded by the F_1, the EP19 subsag is controlled by the F_2 and F_3, the EP20 subsag is determined by the F_4, the EP21 subsag is controlled by F_5 and F_6, and the EP27 subsag is controlled by F_7 and F_8. These boundary faults trend mostly NE-ENE and WNW.

3 Data and methods

Structural features and the spatial distribution of the YYFZ in the PRMB were analyzed through detailed seismic interpretation. All these 3D seismic and well data were acquired by the China National Offshore Oil Corporation (CNOOC) Shenzhen Branch and associated cooperative services companies over the past decades. The seismic profiles nearly cover the whole region of Yangjiang Sag, over 5,600 km^2. The bin size of the survey is 12.5 * 12.5 m. Inline seismic profiles are orientated NW, approximately perpendicular to the basin trend. Standard seismic interpretation workflows for the tectonic-stratigraphic analysis and magmatic body identifications were carried out in Geoframe Open Works (software). A stratigraphic framework was established by integrating 3D seismic and log data with VSP information from some typical wells. Due to its relatively integrated stratigraphic sequence, petroleum exploration boreholes were used to calibrate the Cenozoic strata. Twelve key seismic-stratigraphic boundaries have been identified and named following the nomenclature termed by the CNOOC as T_g (66.5 Ma), T_{82} (42.5 Ma), T_{81} (39.5 Ma), T_{80} (35 Ma), T_{71} (33 Ma), T_{70} (30 Ma), T_{60} (23 Ma), T_{50} (18.5 Ma), T_{40} (15.5 Ma), T_{32} (13.8 Ma), T_{30} (10.5 Ma) and T_{20} (5.5 Ma) (Figure 3). Fault dip and displacement values are calculated on the seismic profiles that cut across the fault (Huang and Liu, 2014). The time-depth conversion was performed using a second-order polynomial, $D=0.000274591t^2+0.72410996t+31.78776360$ (D-depth/m, t-TWT/ms), derived from boreholes within the study area.

The workflow includes the following steps: 1) identify and correlate seismic horizons; 2) generate time structural maps, seismic volume slices, and fault distribution maps during the different seismic reflectors; 3) observe the patterns of en echelon, feather-shaped, horsetail-shaped in map view; 4) observe the stacking patterns of flower-like or Y-shaped structures along the YYFZ; 5) systematically investigate the concomitant changes of depocenters; 6) calculate fault kinematics features; 7) conclude the initial time and evolutionary history of the YYFZ.

Fault geometry features were portrayed based on seismic sections covering the entire study area. Fault orientations are depicted in rose diagrams. Fault kinematics features and their tectonic evolution history were analyzed using 2Dmove software. The evolution history of the YYFZ can be constrained by growth strata and fault assemblage in the profile.

4 Results

The seismic sections across the YYFZ were selected to represent its structural characteristics in the Yangjiang Sag, the northern Kaiping Sag, and the Yunkai Low Uplift. As shown in Figure 5, the YYFZ mainly displays sub-vertical faults, Y-shaped or flower-like structures. In the Yangjiang Sag, the abovementioned structures were primarily observed between the interface T_{70} or T_{80} and T_{32}, while in the northern Kaiping Sag and the Yunkai Low Uplift, they were mainly between T_{80} and T_{32} with a few just between T_g and T_{60} (Figure 5).

4.1 Distribution patterns in map view

4.1.1 Yangjiang sag

Previous studies have suggested that the density of secondary faults can be used to constrain the relative intensity of faults (Huang et al., 2015). Here, we used fault patterns at different seismic reflectors to delineate the distribution and variations in secondary faults in different strata. In the deeper seismic reflectors (Figure 6A), the main faults formed simple NE- and ENE-trending alignments parallel or left-stepping en echelon structures. Subsequently, the formation of a fault system in the early stage may be related to extension, accompanied by slighter dextral transtensional. Besides, these faults only occur in the eastern section, which may be related to the YYFZ as a transfer zone. In contrast, in the middle seismic reflectors, the number, size, and distribution area of the ENE-trending fault become large. Broom-shaped structures and en echelon fault patterns were more extensively developed in the Yangjiang Sag (Figures 6B,C), suggesting that the strike slipping was more intense than in the early Middle Eocene. Meanwhile, a few EW- and WNW–trending faults arose in the sag, especially in its eastern part. The horsetail-shaped structures and right-stepping en echelon fault structure can be identified. The rose diagrams also show that strikes of newborn faults changed from the NE–ENE to the EW-WNW since the Late Eocene, implying a change in the extensional stress from NWN to N–S during the syn-rift stage. In the post-rift stage, the ENE- or NE-trending fault is less active. However, the abundant WNW-or EW-trending faults formed and cut off the pre-existing NE- or ENE-trending faults. These WNW-trending faulting assembled into right-stepping en echelon or horsetail-like patterns (Figure 6D).

The abovementioned characteristics reveal that the YYFZ experienced two tectonic episodes during the Cenozoic: 1) extensional deformation as a transfer zone during the Eocene and 2) sinistral transtensional deformation from the Oligocene to Neogene. Besides, the intensity of the dextral transtensional motion was weak during the early Middle Eocene. Still, it was

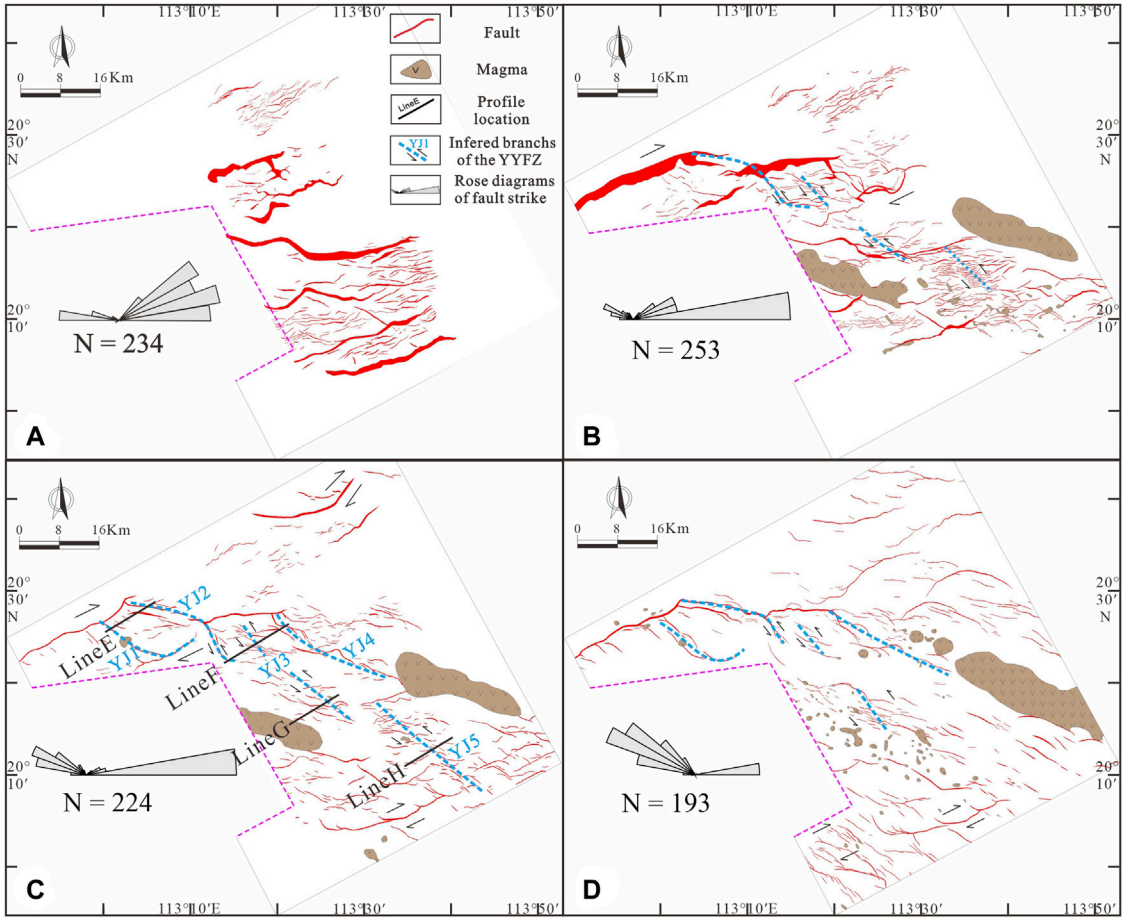

FIGURE 6
Fault patterns in different seismic reflectors of the Yangjiang Sag. **(A)**-T_{82}; **(B)**-T_{80}; **(C)**-T_{70}; **(D)**-T_{40}.

enhanced from the Middle Eocene to the Middle Miocene and became less active in the sag.

4.1.2 Northern kaiping sag

This study area is located in the Kaiping Sag, bounded by the Baiyun Sag to the east, Panyu low Uplift and Shenhu Uplift to the north, and the Yunkai low Uplift to the south (Figure 2). In the sag, the major faults are EW-trending and display simple parallel or right-stepping en echelon structures (Figure 2). Similarly, in the middle seismic reflectors (such as the T_{70} interface), the fault distribution pattern in the northern Kaiping Sag also suggests that the boundary faults are composed of a series of NW- or EW-trending faults. However, they are not continuous and smaller, and display a right-stepping en echelon pattern (Figure 7).

4.1.3 Yunkai low uplift

The Yunkai Low Uplift, mainly distributed along the NW direction, is located in the tectonic transition zone from the Kaiping Sag in the west to the Baiyun Sag in the east (Figure 8). Influenced by the YYFZ, the pre-existing faults experienced strike-slip reactivation, and the Uplift is characterized by WNW-trending right-stepping small-scale normal faults arranged in en echelon pattern (Figure 8). Therefore, to unravel the tectonic evolution of YYFZ, the fault patterns in different seismic reflectors of the Yunkai Low Uplift are carried out. The maps show that the dominant trend of faults in the study area mainly includes NWW/NW, EW, and ENE directions (Figure 9A), which show a clockwise rotation. During the Late Eocene to the Oligocene (corresponding to the T_{80}-T_{70} in space, ~35–30 Ma in time), the main faults in the Yunkai Low Uplift were WNW/NW-trending and short with curved or sigmoidal features (Figure 9B). They were different from the NEE-trending main faults in the northern depression zone, such as the Yangjiang Sag. The horsetail- or right-stepping fault patterns in the Yunkai Low Uplift can be seen (Figures 9B,C), which suggests slighter sinistral transtension. Compared with the deeper sector, the number, size, and distribution area of the WNW-/NW-trending faults in the shallow seismic reflectors

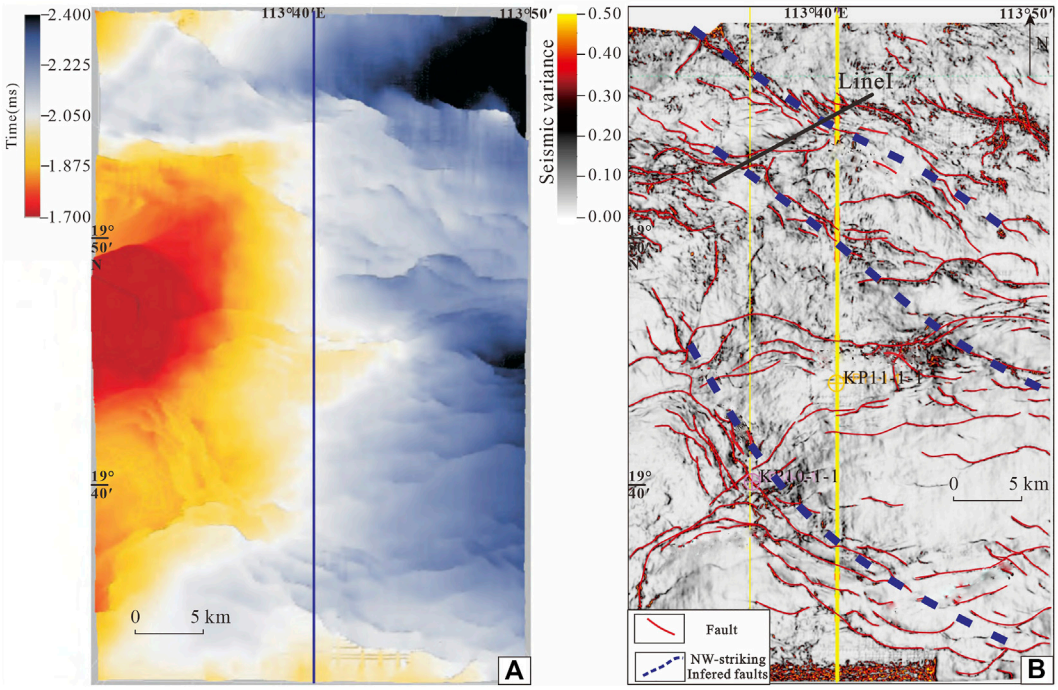

FIGURE 7
Distribution characteristics of fault plane combination along T_{70} in the northeastern part of the Kaiping Sag (Figure 2 shows figure location). **(A)**. T_0 plane map; **(B)** Two-dimensional fracture plane distribution along the coherent attribute recognition (revised from Wang et al., 2021a; Wang et al., 2021b).

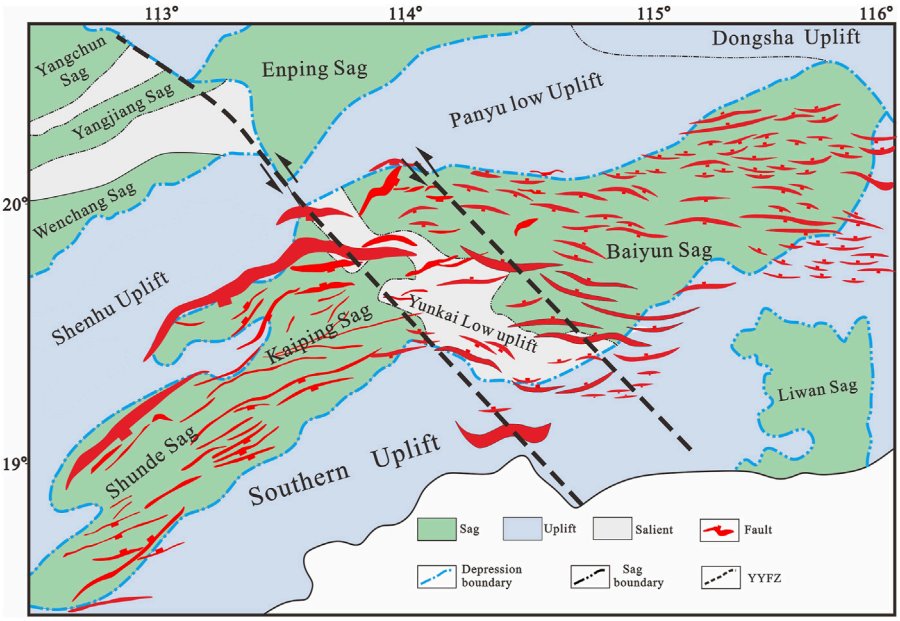

FIGURE 8
Structural units and fault pattern in the Zhu II Depression. The WNW- and E-W-trending secondary faults are assembled to produce an en echelon fault pattern in the T_{80} interface. Figure location is shown in Figure 2 (revised from Wang et al., 2021).

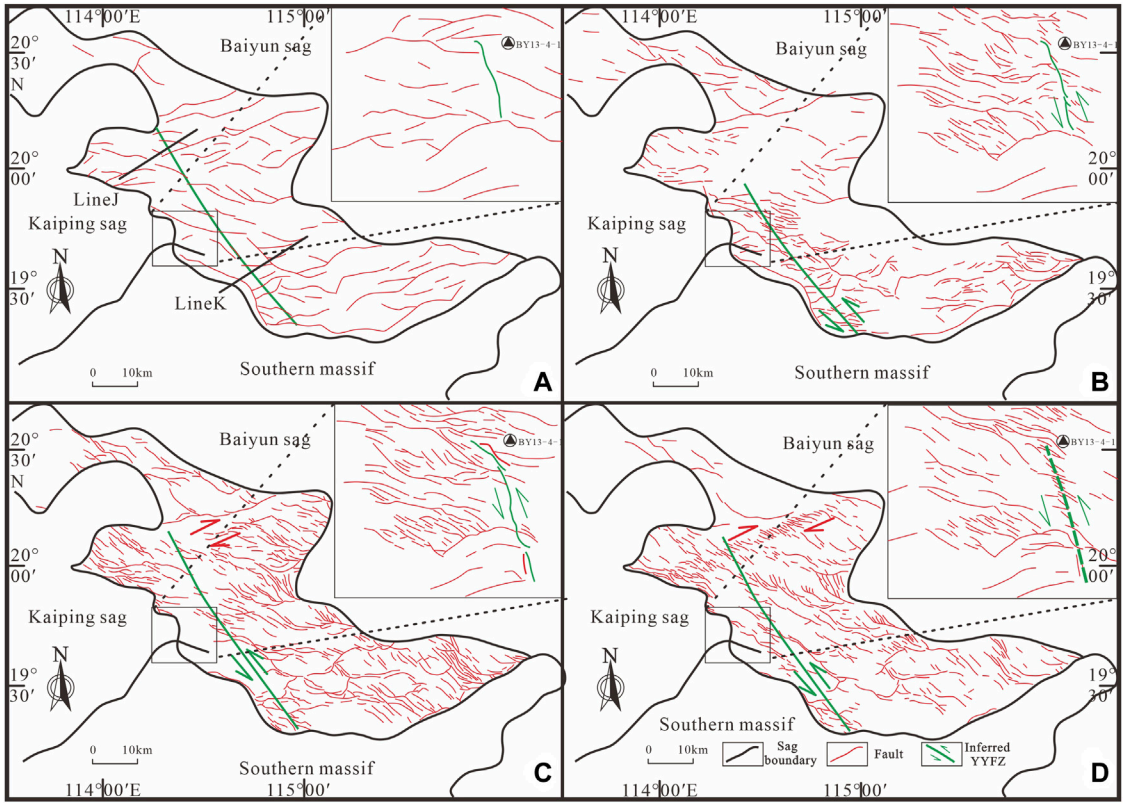

FIGURE 9
Fault patterns in different seismic reflectors of the Yunkai low uplift (revised from Sun et al., 2014; Yu et al., 2021). **(A)**-T_g; **(B)**-T_{80}; **(C)**-T_{60}; **(D)**-T_{40}.

become smaller (Figures 9C,D). Besides, a group of NW-trending minor faults at the interface T_{40} exhibits a left-stepping en echelon pattern, suggesting ENE-trending dextral transtensional motion (Figure 9D).

Similarly, the strike-slip motion is evident in the BY13 area southwest corner of the Yunkai Low Uplift. During the early faulting, these NW-trending faults were reactivated as normal faults (Figure 9A). Compared with the T_g interface, the fault appears as discontinuous linear structures from the Late Eocene to the Early Miocene (T_{80}-T_{60} in space; Figures 9B,C). Meanwhile, these WNW-trending secondary faults developed along the NW-trending fault's right side and converged to the main faults. In comparison, the upper faults at interface T_{40} are composed of a series of WNW-trending faults, which present right-stepping en echelon arrangement (Figure 9D).

4.2 Structure styles in sections

4.2.1 Yangjiang sag

The profiles crossing the Yangjing Sag indicate that the NE-NEE trending faults determine the structural framework of the subbasin. As the main fault of the study area, the NEE-trending F_1 and F_4 faults present as a listric fault with a large offset. Notably, a series of WNW-trending secondary faults began to develop in the E_2e depositional stage. Some of them form flower-like or Y-shaped structures, indicating transtensional deformation characteristics.

To reveal the profile features of those WNW-trending secondary faults from north to south, we chose four SWW–NEE typical seismic profiles in the Yangjiang Sag (Figure 10, LineE-H). Profiles reveal that the NW-trending YJ1, YJ2, YJ3, YJ4, and YJ5 faults display a geometric feature similar to a steeply dipping listric fault in the lower part but a negative flower or Y-shaped structure in the upper part (this is, the lower listric upper flower structure) (Figure 10). These faults penetrate the T_{80} or T_g unconformity, terminate below the T_{32} (Figure 10), and control non-wedge-like sedimentation. Among those faults, the YJ2 fault in the north segment is mainly west dipping, and those in the south segment are mainly east dipping (Figure 10, LineE, and F), which display ribbon effect (Romeo et al., 2005) in space. Similarly, the YJ3 fault in the north segment is mainly east-dipping, and those in the south segment are mainly west-dipping (Figure 10, LineF, and G).

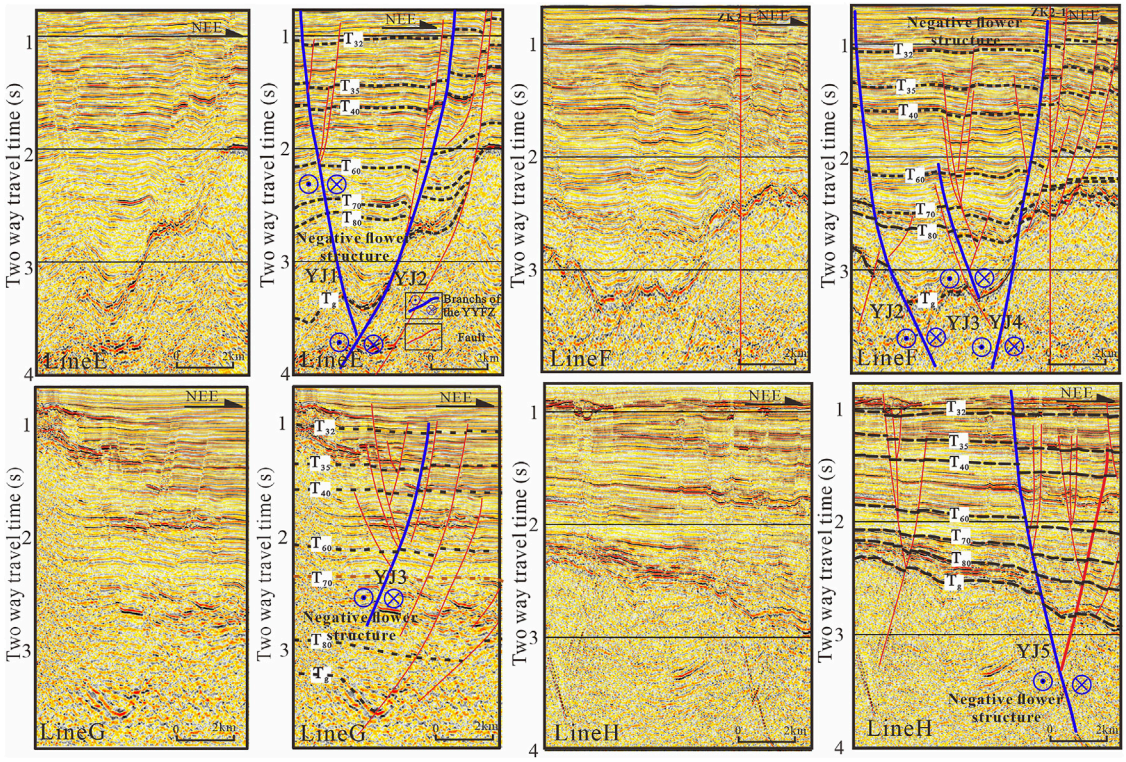

FIGURE 10
Interpreted seismic profiles showing fault intersections in the Yangjiang Sag. Profile locations are shown in Figure 6C. The profiles reveal that the NW-trending faults are characterized by flower-like structures that indicate they experienced transtensional deformation.

4.2.2 Northern kaiping sag

The basement-involved faults in the northern Kaiping Sag are mainly planar or shovel-type faults at a high angle. Notably, a set of new normal faults began to develop during the depositional stage of E_2e. Some of them form flower-like or Y-shaped structures with main faults. Besides, magmatic diapirs intruded into the sedimentary cover of the basin along these faults and even erupted over the seabed. According to growth strata and fault assemblage in the profile (Figure 11, Line I), a displacement of normal fault or transtensional fault occurred in the basement-involved faults in the E_2e-E_3z depositional stage.

4.2.3 Yunkai low uplift

As the transition zone between the two sags, the Yunkai Low Uplift connects the Kaiping Sag and the Baiyun Sag with a slope and a faulted step zone, respectively (Figure 2). On the Yunkai Low Uplift, the Wenchang Formation is mostly eroded, directly overlain by the Enping Formation. Inside the Uplift, various scales of listric and planar normal faults develop. Several normal fault combinations display asymmetrical negative flower structures (Figure 11, LineJ, and K). The deep layer structure is characterized by a listric fault through the T_g interface and developed upward across the T_{80} interface.

4.3 Characteristics of the sedimentary succession

Sequence thicknesses in different stages reveal three-stage depocenter migration, indicating two-stage structural transitions in the study area. There developed five independent depocenters during the depositional stage of E_2w, forming YJ24, EP19, EP20, EP21, and EP27 subsags, respectively (Figure 12A). In this period, these subsags were mainly controlled by the main faults (such as F_1, F_4, F_6, and F_7) obviously, and the center of the E_2w sequence is distributed primarily in the east of the sag with the characteristics of thick in the east and thin in the west. However, during the depositional stage of E_2e^L, the depocenter migrated to the west Yangjiang Sag for the first time; the EP19 and YJ24 subsags presented, leading to thick in the west and thin in the east. Furthermore, from E_2e^L to E_3z, the study area presents a westward thickening slope and their depocenters are located along the NWW-trending faults and align in a right-stepping en echelon pattern, indicating that the NW-trending faults were sinistral during the depositional stage of E_2e^L-E_3z (Figures 12B–D). The depocenter migration is probably consistent with the intense activity of the strike-slip faults.

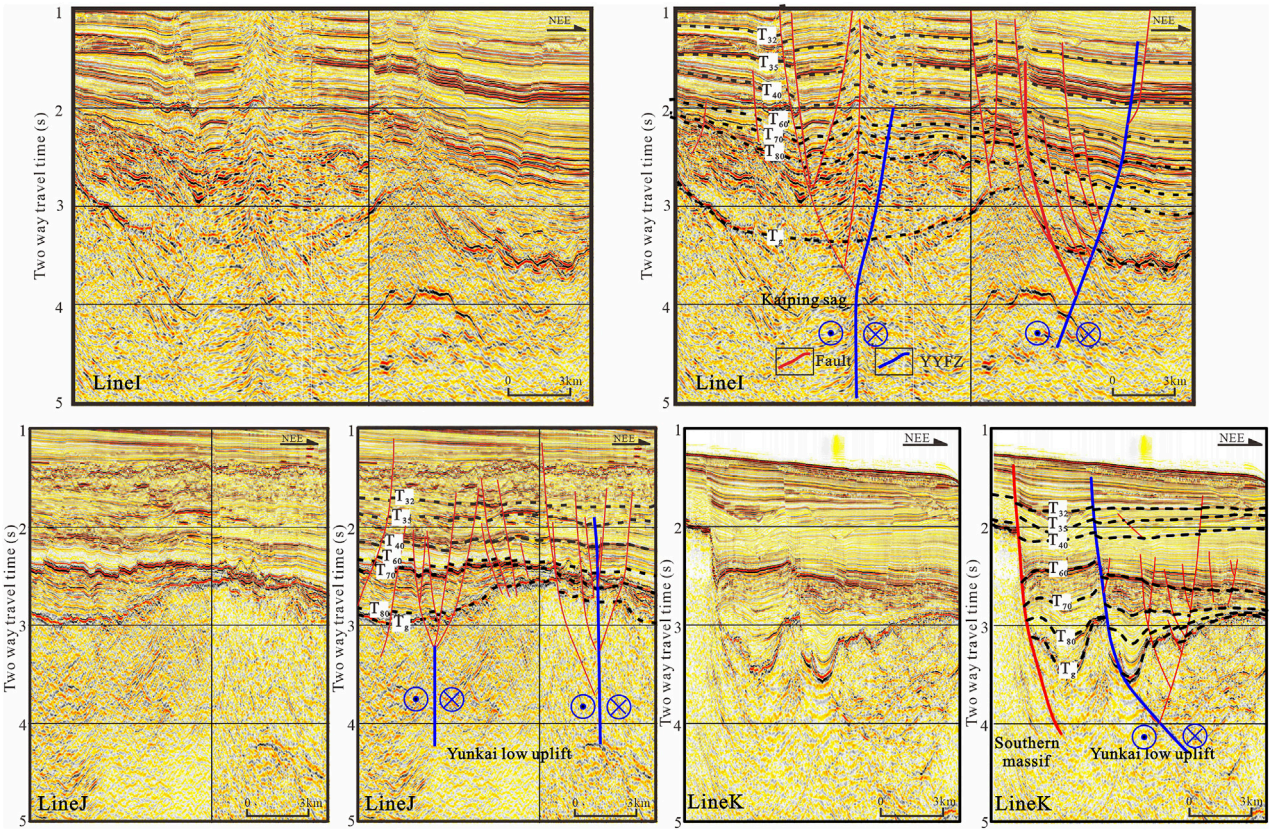

FIGURE 11
Seismic profiles show the geometry of the NW-trending faults in the northern Kaiping Sag and Yunkai low uplift. The location of seismic profiles Line I and Line J-K are demonstrated in Figures 8, 9, respectively. These faults are characterized by flower or Y-shaped structures.

Based on the analyses presented above, the residual thickness of E_2w, E_2e, and E_3z showed an obvious counter-clockwise rotation of the depocenter orientations from ENE to WNW in the Yangjiang Sag; a similar depocenter rotation also occurred in the Yunkai Low Uplift at the same time (Yu et al., 2021). Consequently, it indicates a clockwise rotation of the extension stress field from NW (in the E_2w depositional stage) to S-N (in the E_2e depositional stage), consistent with the stress field rotation in the PRMB (Hao et al., 2021).

5 Discussion

5.1 Initiation of the sinistral motion of the YYFZ

Several distinctive structures were used to identify the YYFZ in the PRMB. These structures include 1) a high-subvertical dip angle (Harding, 1990) or a Y-shaped structure governed by steeply dipping faults and a flower structure in cross-section (Harding, 1985; Cheng et al., 2017; Han et al., 2017), 2) the abrupt changes of the thickness of the same lithologic stratigraphic unit, the sedimentary facies, and the formation occurrence across fault planes in the section (Ghalayini et al., 2014), 3) linear geometry, en echelon faults, pull-apart structures, and horsetail splays in the map view (Harding, 1985; Mcclay, 2001); dolphin (Graham et al., 1984) and ribbon effects (Romeo et al., 2005) in space. Previous results have shown that the blind fault and tectonic trend zones in sedimentary layers would inherit from pre-existing faults when suffering deformation (Bellahsen and Daniel, 2005; Wang et al., 2015). These pre-existing structures incline to show strike-slip deformation, accompanying many minor faults aligning in a parallel or en echelon arrangement (Liu Y et al., 2021). In this study, the YYFZ exhibited en echelon arrays of minor faults in the map view and flower-like or Y-shaped structures in the section. These small-scale normal faults are arranged in a right-stepping en echelon pattern on the T_{80} seismic interface, indicating that the YYFZ has a consistent initiation time (i.e., at about 35 Ma) and has the same overall kinematic framework. The fault plan arrangements suggest that these NW or WNW-trending faults had experienced sinistral

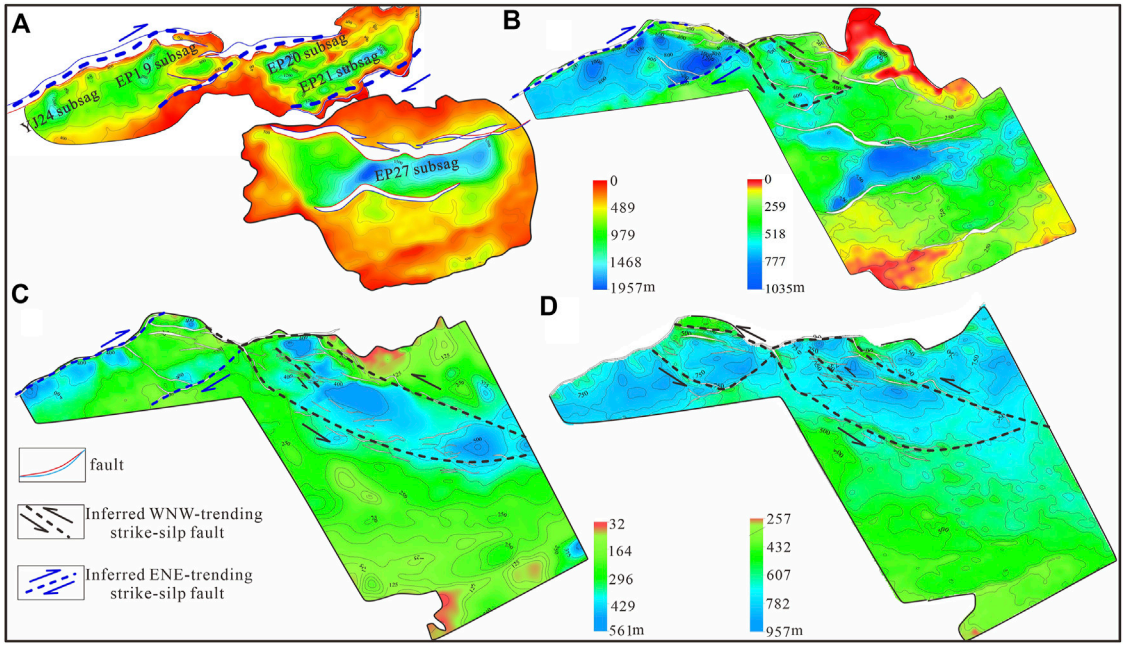

FIGURE 12
Sequence characteristics of different periods in the Yangjiang Sag area. **(A)**, **(B)**, **(C)**, and **(D)** show the thickness of the E_2w, E_2e^U, E_2e^L, and E_3z Formation, respectively. Note the depocenter migration in **(B)** and **(C)**.

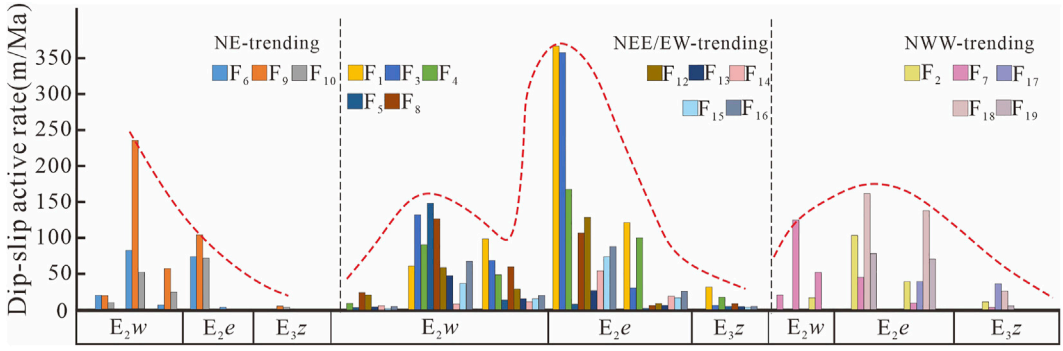

FIGURE 13
Average rates of active dip-slip faulting of main faults in the Yangjiang Sag.

strike-slip motion. Besides, the syn-depositional fault map of Paleogene shows that the E_2e^L sequence presents a thickening slope westward, and the depocenters are located in the NWW trending faults, which also confirms that the NW-trending strike-slip faults began to slightly motion during the stage (Figure 12B). Based on the fault pattern in the BY13 area, Sun et al. (2014) indicated that the NW-trending shear faults acted sinistrally about 32 Ma. Wang et al. (2013) also proposed that the sinistral transtensional activities occurred during the middle to early Oligocene, according to a comprehensive interpretation of seismic stratigraphic sequence and faults.

It is difficult to track the activity history because the strike-slip faults move along the strike (Yu et al., 2008). However, the activity of secondary faults derived from the main strike-slip faults can reveal the tectonic activity of strike-slip faults. By calculating the activity rate of main faults in the Yangjiang Sag during the Paleogene, the results reveal that the NE/ENE-trending normal faults activated during the depositional stage of E_2e and reached the peak stage during the period of the E_2e^L sequence. Meanwhile, the WNW-trending faults related to the YYFZ are active during the depositional stage of E_2e (Figure 13), which may also suggest that the YYFZ began to be active during the period.

As mentioned above, we suggest that all these fault bends or en echelon structures were induced by the sinistral strike-slip motion of the YYFZ, indicating that the sinistral slip of the YYFZ commenced at about 35 Ma.

5.2 Cenozoic evolutionary history of the YYFZ

Much previous work has shown that the Meso-Cenozoic evolution of the YYFZ was characterized by huge and significant sinistral motion (Zhan et al., 2021; Mu et al., 2022; Wang et al., 2022), whereas its Cenozoic evolutionary history is poorly known.

Evidence of the sense of motion from flower-like structures in the profile and en echelon arrangement in the plane along the YYFZ indicate that the Cenozoic sinistral motion occurred around 35 Ma. The fault pattern in the plane and the main fault cut through in the strata above maker T_{80} in the profile show that their remarkable formation period was during the depositional stage of E_2e–N_1z (T_{80}-T_{40} in space), indicating sinistral motion of the YYFZ during the period (Figures 5, 6). Remarkably, the change of tectonics stress regime and sediment provenance before and after the T_{80} reflection interface occurred in the PRMB (Tang et al., 2020), which is further validated by the fact that the EW-trending normal faults are primarily developed in the Yangjiang Sag (Figure 6B). Besides, combined with the sedimentary thickness data, the Yangjiang Sag is a strike-slip pull-apart superimposed area composed of multiple WNW-trending faults in the E_2e-E_3z depositional stage, displaying en echelon arrangement itself to some extent as well (Figures 13B–D). These features strongly confirm that the YYFZ was active during these two periods. One further point should also be emphasized, although the depocenter appears not obvious in Neogene strata, some en echelon subsidiary faults are nevertheless still developed among shallow strata (Figure 6D), indicating that strike-slip motion still occurred during Neogene but has become much weaker.

The kinematics characteristics of the YYFZ in the Eocene remain controversial; some workers suggest that the YYFZ showed dextral displacement in the earlier faulting stage, which subsequently results in the boundary fault right laterally displaced (Lv et al., 2017); however, other authors proposed that the NW-trending pre-existing faults probably reactivated only as a transform zone under the NW-SE oriented stress field, regulating the differential tectonic deformation on both sides (Zhan et al., 2021; Shen et al., 2022). The transform zone is characterized by transform fault, which links different segments of extensional structural domains (Chen et al., 2011). Remarkably, the YYFZ in the Yangjiang Sag, as a transfer zone, accommodates the differential tectonic deformation on both sides (such as F_1 and F_6) during the depositional stage of E_2w. Moreover, the SW-NE-directed seismic profiles cross YYFZ in the Yunkai Low Uplift show that the listric-shaped or flat-shaped faults and graben-like basins are primarily identified during the early Eocene to the middle Eocene, indicating that faults are mainly derived from the extensional activity.

Many investigations on the post-rift stage faults in the PRMB (Sun et al., 2014; Wu et al., 2014; Zhou et al., 2020) show that the number of subsidiary normal faults related to the sinistral shear of the YYFZ decreased greatly after 13.8 Ma and distributed more concentrated in NWW direction at shallow levels. Besides, the strike-slipping of the YYFZ controlled the distribution of magma activities in the western PRMB from 23.6–10 Ma, considering that nearly all the igneous rocks were distributed along the YYFZ (Li G et al., 2022).

According to the above discussions, we propose a new Cenozoic evolutionary history of the YYFZ (Figure 14). After a long period and significant sinistral motion during the Mesozoic, the YYFZ was reactivated as a transfer zone as a whole during 65–35 Ma. Besides, the principal deformation zone along the NE-trending strike-slip fault controlled the development of a series of Paleogene half-grabens (Cheng et al., 2012; Li et al., 2012; Wang W et al., 2017; Wang et al., 2020; Wang et al., 2021; Zhan et al., 2021). A sinistral shear with a component of extensional deformation from 35 to 16.5 Ma; meanwhile, the sinistral motion was most intense from 21 to 16.5 Ma. After 16.5 Ma, the SCS stopped the seafloor spreading, and the whole area entered a thermal subsidence period (Sun et al., 2008). In this period, the activity of YYFZ maintained the previous sinistral motion and the activity intensity decreased.

5.3 Implication for regional tectonic evolution and geodynamics of SCS

During the Paleogene (ca. 65–55 Ma), the Pacific plate subducted beneath the Eurasian continent and interacted with mantle materials, which probably resulted in slab retreat of the Pacific Plate and subsequently induced the initial rifting in PRMB (Allen et al., 1998; Liu et al., 2017; Ren, 2018; Wang et al., 2020; Wang et al., 2021). During this period, the rifting activities occurred only in the northern depression zone (Wenchang Sag in the Zhu III depression and Lufeng Sag of Zhu I depression), and the study area (the Yangjiang Sag and the Yunkai Low Uplift) was an uplift area. Subsequently, accompanied by the constant slab retreat of the Pacific Plate (Müller et al., 2008), several NE/ENE-trending syn-depositional faults widely developed in the PRMB during the early Eocene to the early middle Eocene (ca. 55-44 Ma), such as Yangjiang Sag, which exhibited listric-shaped or flat-shaped patterns on seismic profiles and dominated graben-like basins (Figure 15A).

During the late Middle Eocene to the Early Miocene (ca. 44-21 Ma), the Indian Plate continued to move northeastwards with a gradually declining plate velocity (Lee and Lawver, 1995;

Formation	Member	Age of the bottom(Ma)	Proposed evolution history of the YYFZ	Principle driving force	Evolutionary stage of the basin
Quaternary	Q	1.9			post-rift stage
Wanshan	N_2w	5.5	sinistral shear with a component of extensional deformation		
Yuehai	N_1y	10.5		WNW-ward subduction of the Philippine Sea Plate & the extrusionsion of the Indochina Block	
Hanjiang	N_1h	16.5	Stronger sinistral shear with a component of weak extensional deformation		
Zhujiang	N_1z	21			
Zhuhai	E_3z	30	sinistral shear with a component of extensional deformation	Westward subduction of the Pacific Plate & the extrusionsion of the Indochina Block & the slab-pull system of the proto-SCS	Rift stage
Enping	E_2e	35			
Wenchang	E_2w	66.5	Transfer zone(with extensional deformation)		

FIGURE 14
Cenozoic evolution history of the YYFZ (revised from Huang et al., 2015).

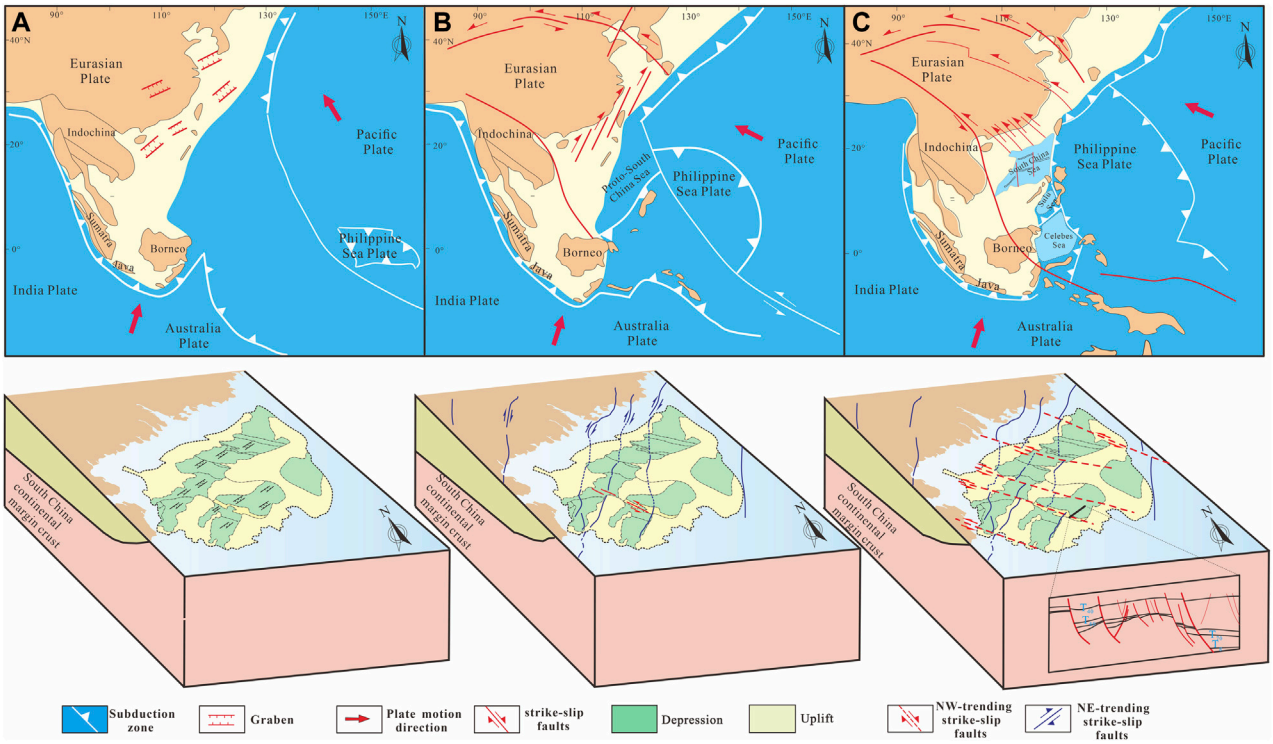

FIGURE 15
Simplified model showing three-stage extension and geodynamics in the Cenozoic PRMB (revised from Hall, 2012; Li S et al., 2022; Wang et al., 2022). **(A)**-55 Ma; **(B)**-35 Ma; **(C)**-20 Ma.

Torsvik et al., 2008). Simultaneously, to the east of the SCS, the subduction direction of the Pacific Plate changed from NNW to WNW, and the subduction velocity of the Pacific Plate to Eurasia increased from 38 mm/yr to 90 mm/yr (Northrup et al., 1995; Copley et al., 2010), to the south of the SCS, the S-directed slab-pull force of the proto-SCS began to affect the continental margin of the SCS. Eventually, the common effect among these three dynamic systems probably leads to a dextral trans-extensional stress field. Therefore, the NE-trending faults changed from normal to right-lateral strike-slip faults and were mainly active in the PRMB (Figure 15B; Wang et al., 2021). Besides, the dextral activity of the NE-trending fault has a

significant impact on the structure evolution of the PRMB (Mu et al., 2022; Zhou et al., 2022). Influenced by the dextral shear activity, the subsidence center of the Yangjiang Sag and the syn-depositional faults were primarily NEE-trending during this stage.

It is generally agreed that the Red River Fault (RRF) experienced an earlier sinistral deformation (e.g., Tapponnier et al., 1990; Leloup et al., 1995) and a later dextral movement (e.g., Clift and Sun, 2006; Sun et al., 2009; Sibuet et al., 2016). However, the timing of sinistral shear deformation is still a controversial topic. Most geologists suggested that the onset of the sinistral shearing activity along the Red River Fault occurred at ~35 Ma (Leloup et al., 1995; Sun et al., 2003; Clift and Sun, 2006; Liang et al., 2007; Zhu M et al., 2009; Zhao Z et al., 2018; Wang et al., 2019). However, some studies implied that the sinistral shearing deformation occurred much later, at 30–21 Ma (e.g., Cao et al., 2011; Liu et al., 2012, 2015; Tang et al., 2013). In this study, we suggest that the sinistral motion of the YYFZ has started since the formation of T_{80} interfaces (about 35 Ma), which is consistent with the initiation time of the RRF proposed by Lei et al. (2021). Thus, we infer that these faults probably have a consistent initiation time (at about 35 Ma).

At this moment, the Pacific Plate subducted beneath the Eurasia Plate with a high speed of 80 mm/yr to the east (Northrup et al., 1995); more importantly, the rapid extrusion of the Indochina block induced by the Indian-Asian collision occurred to the west (Lee and Lawver, 1995; Zhang et al., 2013; Guo et al., 2022; Wang et al., 2022). Besides, it is worth noting that the S-directed slab-pull force of the proto-SCS also plays an important role (Hall, 2013; Madon et al., 2013). Influenced by the joint action among these three dynamic systems and the secondary shear stress field trigged by the NE trending strike-slip fault (Zhou et al., 2022), the NW-trending faults in the northern SCS were reactivated subsequently, creating a series of en echelon arrays of minor faults and flower-like structures at depth (Zhang et al., 2019; Liu Y et al., 2021), where a conspicuous blind fault zone developed, similar to the NW-trending YYFZ in this study. Following the renewed north-south extension in the South China continental margin, the SCS spreading began at 34 Ma or 32 Ma (Li C.-F et al., 2014), resulting in the concentration of extensional stress sharply on the oceanic ridge.

After the Miocene (ca. 21-0 Ma), the SCS began to subduct along the Manila Trench and affect the adjacent tectonic domains (Gao et al., 2018). At the same time, the Philippine Plate was subducting in the WNW direction (Yan et al., 2022), and the Indian Plate continued to move northeastwards. The joint effect resulted in continuous sinistral motion of the NW-trending faults. In contrast, the NE-trending faults were not active or slightly active (Figure 15C). Above all, the three-stage evolution of the faults in the study area is an outcome of the basin evolution, which is closely associated with the movement of surrounding plates.

6 Conclusion

Based on the fault system maps and seismic profiles, we systematically investigated the development characteristics of the fault system in the western PRMB and can make the following conclusions:

1. A series of EW- and WNW–trending faults arose in the E_2e depositional stage, which exhibit horsetail and en echelon structures in the map view and flower-like or Y-shaped structures in the profile. Together with the response of depocenters in the Yangjiang Sag adjacent to the YYFZ, we suggest that the YYFZ have a consistent initiation time (i.e., at about 35 Ma).

2. Combined with the Cenozoic evolution of the PRMB, the Cenozoic activity of the YYFZ includes the following three stages: 1) 65-35 Ma, the YYFZ was a first-order transfer zone accommodating significant intraplate extensional deformation; 2) 35–16.5 Ma, the YYFZ displays as a sinistral strike-slip fault zone; 3) after 16.5 Ma, the activity of YYFZ maintained the previous sinistral motion and tended to be weakened.

3. The evolution of the PRMB in the late stage is affected by strike-slip reactivation along the YYFZ. This reactivation may be related to the joint action among the rapid extrusion of the Indochina block induced by the Indian-Asian collision to the west, the subduction of the Pacific Plate beneath the Asia continent to the east, and the slab-pull system of the proto-SCS to the south.

Data availability statement

The original contributions presented in the study are included in the article/supplementary material, further inquiries can be directed to the corresponding authors.

Author contributions

HZ processed the data, wrote the manuscript and designed the figures. GW and YS conceptualized the study and performed the analysis of the manuscript. GP, XD and DZ provided data sources and helped revise the manuscript. PW, JZ, and SL supervised the study. SL, PW, and GW acquired the funding.

Funding

This work was Financially supported by the Marine S&T Fund of Shandong Province for Pilot National Laboratory for Marine Science and Technology (Qingdao) (No. 2022QNLM050302), National Natural Science Foundation of China (Grant Nos. 42121005, 91958214, 42072235, 42002220), Shandong Provincial Natural Science Foundation (No. ZR2021ZD09), 111 Project (Grant No. B20048).

Conflict of interest

Authors GP, XD and DZ were employed by the Shenzhen Branch, CNOOC China Limited.

The remaining authors declare that the research was conducted in the absence of any commercial or financial relationships that could be construed as a potential conflict of interest.

Publisher's note

All claims expressed in this article are solely those of the authors and do not necessarily represent those of their affiliated organizations, or those of the publisher, the editors and the reviewers. Any product that may be evaluated in this article, or claim that may be made by its manufacturer, is not guaranteed or endorsed by the publisher.

References

Allen, M. B., Macdonald, D. I. M., Xun, Z., Vincent, S. J., and Brouet-Menzies, C. (1998). Transtensional deformation in the evolution of the Bohai Basin, northern China. *SP* 135, 215–229. doi:10.1144/GSL.SP.1998.135.01.14

Bellahsen, N., and Daniel, J. M. (2005). Fault reactivation control on normal fault growth: An experimental study. *J. Struct. Geol.* 27, 769–780. doi:10.1016/j.jsg.2004.12.003

Cai, G., Zhang, X., Peng, G., Wu, J., Liu, B., Bai, H., et al. (2021). Neogene volcanism and tectonics along the yangjing-yitong'ansha Fault Zone in the northern south China sea margin. *Geotect. Metallogenia* 45, 40–52. doi:10.16539/j.ddgzyckx.2021.01.004

Camanni, G., and Ye, Q. (2022). The significance of fault reactivation on the Wilson cycle undergone by the northern South China Sea area in the last 60 Myr. *Earth-Science Rev.* 225, 103893. doi:10.1016/j.earscirev.2021.103893

Cao, J., Xia, S., Sun, J., and Xu, H. (2014). Comparison of fault structure characteristics in the northern Pearl River Mouth Basin and its geological implication. *Prog. Geophys.* 29, 2364–2369. doi:10.6038/pg20140555

Cao, S., Neubauer, F., Liu, J., Genser, J., and Leiss, B. (2011). Exhumation of the Diancang Shan metamorphic complex along the Ailao Shan-Red River belt, southwestern yunnan, China: Evidence from 40Ar/39Ar thermochronology. *J. Asian Earth Sci.* 42, 525–550. doi:10.1016/j.jseaes.2011.04.017

Chen, F., Wang, X., and Chen, Z. (2011). Analysis of transform structures in extensional fault depressions. *Geoscience* 25, 617–625. doi:10.3969/j.issn.1000-8527.2011.04.001

Chen, H., Wu, X., Zhou, D., Wang, W., and Hao, H. (2005). Meso-cenozoic faults in Zhujiang River Mouth basin and their geodynamic background. *J. Trop. Oceanogr.* 24, 52–61. doi:10.3969/j.issn.1009-5470.2005.02.007

Cheng, S., Li, S., Suo, Y., Liu, X., Yu, S., Dai, L., et al. (2012). Cenozoic tectonics and dynamics of basin groups of the northern South China Sea. *Mar. Geol. Quat. Geol.* 32, 79–93. doi:10.3724/SP.J.1140.2012.06079

Cheng, X., Zhang, Q., Yu, X., Du, W., Liu, R., Bian, Q., et al. (2017). Strike-slip fault network of the Huangshi structure, SW Qaidam Basin: Insights from surface fractures and seismic data. *J. Struct. Geol.* 94, 1–12. doi:10.1016/j.jsg.2016.10.011

Clift, P. D., and Sun, Z. (2006). The sedimentary and tectonic evolution of the Yinggehai-Song Hong basin and the southern Hainan margin, South China Sea: Implications for Tibetan uplift and monsoon intensification. *J. Geophys. Res.* 111, 1–28. doi:10.1029/2005JB004048

Copley, A., Avouac, J.-P., and Royer, J.-Y. (2010). India-Asia collision and the Cenozoic slowdown of the Indian plate: Implications for the forces driving plate motions. *J. Geophys. Res.* 115, B03410. doi:10.1029/2009JB006634

Fu, C., Li, S., Li, S., and Xu, J. (2021). Spatial and temporal variability of sediment infilling and episodic rifting in the north Pearl River Mouth basin, south China sea. *J. Asian Earth Sci.* 211, 104702. doi:10.1016/j.jseaes.2021.104702

Gao, J., Wu, S., Yao, Y., Chen, C., Song, T., Wang, J., et al. (2018). Tectonic deformation and fine structure of the frontal accretionary wedge, northern Manila subduction zone. *Chin. J. Geophys.* 61, 2845–2858. doi:10.6038/cjg2018L0461

Ge, J., Zhao, X., Tan, M., Zhuo, H., Liu, C., and Jones, B. G. (2022). Sequence stratigraphy and depositional evolution of the north-eastern shelf (33.9–10.5 Ma) of the Pearl River Mouth basin, south China sea. *Mar. Petroleum Geol.* 141, 105697. doi:10.1016/j.marpetgeo.2022.105697

Ge, J., Zhu, X., Zhao, X., Liao, J., Ma, B., and Jones, B. G. (2020). Tectono-sedimentary signature of the second rift phase in multiphase rifts: A case study in the Lufeng depression (38–33.9 Ma), Pearl River Mouth basin, south China sea. *Mar. Petroleum Geol.* 114, 104218. doi:10.1016/j.marpetgeo.2020.104218

Ghalayini, R., Daniel, J.-M., Homberg, C., Nader, F. H., and Comstock, J. E. (2014). Impact of Cenozoic strike-slip tectonics on the evolution of the northern Levant Basin (offshore Lebanon): Cenozoic tectonics of the Levant basin. *Tectonics* 33, 2121–2142. doi:10.1002/2014TC003574

Graham, S., McCloy, C., Hitzman, M., Ward, R., and Turner, R. (1984). Basin evolution during change from convergent to transform continental margin in central California. *Am. Assoc. Pet. Geol. Bull.* 68, 233–249. doi:10.1306/AD460A03-16F7-11D7-8645000102C1865D

Guo, L. L., Li, S. Z., Zhao, S. J., Zhang, G. X., Suo, Y. H., Liu, H., et al. (2016). Final breakup of continental block and opening of oceanic lithosphere: Insights from deep crustal structure and tectonic evolution of the ocean-continent transition zone in the northern south China sea: OCT zone in the northern SCS. *Geol. J.* 51, 318–330. doi:10.1002/gj.2842

Guo, X., Li, C., Gao, R., Li, S., Xu, X., Lu, Z., et al. (2022). The India-Eurasia convergence system: Late Oligocene to early Miocene passive roof thrusting driven by deep-rooted duplex stacking. *Geosystems Geoenvironment* 1, 100006. doi:10.1016/j.geogeo.2021.09.005

Hall, R. (2012). Late Jurassic–Cenozoic reconstructions of the Indonesian region and the Indian Ocean. *Tectonophysics* 570–571, 1–41. doi:10.1016/j.tecto.2012.04.021

Hall, R. (2013). Contraction and extension in northern Borneo driven by subduction rollback. *J. Asian Earth Sci.* 76, 399–411. doi:10.1016/j.jseaes.2013.04.010

Han, X., Deng, S., Tang, L., and Cao, Z. (2017). Geometry, kinematics and displacement characteristics of strike-slip faults in the northern slope of Tazhong uplift in Tarim basin: A study based on 3D seismic data. *Mar. Petroleum Geol.* 88, 410–427. doi:10.1016/j.marpetgeo.2017.08.033

Hao, S., Mei, L., Shi, H., Paton, D., Mortimer, E., Du, J., et al. (2021). Rift migration and transition during multiphase rifting: Insights from the proximal domain, northern South China Sea rifted margin. *Mar. Petroleum Geol.* 123, 104729. doi:10.1016/j.marpetgeo.2020.104729

Harding, T. P. (1990). Identification of wrench faults using subsurface structural data criteria and pitfalls. *Am. Assoc. Pet. Geol. Bull.* 74 (10), 1590e1609. doi:10.1306/0C9B2533-1710-11D7-8645000102C1865D

Harding, T. P. (1985). Seismic characteristics and identification of negative flower structures, positive flower structures, and positive structural inversion. *Am. Assoc. Pet. Geol. Bull.* 69 (4), 582e600. doi:10.1306/AD462538-16F7-11D7-8645000102C1865D

He, Y., Mei, L., Shi, H., Shu, Y., and Chen, Y. (2019). Structural characteristics and genetic model of the low-angle fault depression:a case in Enping Depression of Pearl River Mouth Basin. *Mar. Orig. Pet. Geol.* 23 (3), 73–81. doi:10.3969/j.issn.1672-9854.2018.03.008

Ho-Shing, Y. (1990). The Pearl River Mouth basin: a rift basin and its geodynamic relationship with the southeastern Eurasian margin. *Tectonophysics* 183, 177–186. doi:10.1016/0040-1951(90)90415-5

Hou, D., Pang, X., Xiao, J., Zhang, J., Shi, H., Wang, J., et al. (2008). Geological and Geochemical evidence on the identification of natural gas migration through fault system, Baiyun sag, Pearl River Mouth basin, China. *Earth Sci. Front.* 15, 81–87. doi:10.1016/S1872-5791(08)60041-X

Hu, D., Zhou, D., Wu, X., He, M., Pang, X., and Wang, Y. (2009). Crustal structure and extension from slope to deepsea basin in the northern South China Sea. *J. Earth Sci.* 20, 27–37. doi:10.1007/s12583-009-0003-6

Huang, K., Zhong, G., He, M., Liu, L., Wu, Z., and Liu, X. (2018). Growth and linkage of a complex oblique-slip fault zone in the Pearl River Mouth basin, northern south China sea. *J. Struct. Geol.* 117, 27–43. doi:10.1016/j.jsg.2018.09.002

Huang, L., and Liu, C. (2014). Evolutionary characteristics of the sags to the east of Tan–Lu Fault Zone, Bohai Bay Basin (China): Implications for hydrocarbon

exploration and regional tectonic evolution. *J. Asian Earth Sci.* 79, 275–287. doi:10.1016/j.jseaes.2013.09.031

Huang, L., Liu, C., and Kusky, T. M. (2015). Cenozoic evolution of the tan–Lu Fault Zone (east China)—constraints from seismic data. *Gondwana Res.* 28, 1079–1095. doi:10.1016/j.gr.2014.09.005

Hui, G., Zhang, P., Li, Z., Wang, W., Hu, L., Li, G., et al. (2022). Opening of the South China sea marginal basin: Insights from the tectonic evolution of the ENE-striking littoral Fault Zone. *Mar. Petroleum Geol.* 145, 105854. doi:10.1016/j.marpetgeo.2022.105854

Lee, T.-Y., and Lawver, L. A. (1995). Cenozoic plate reconstruction of the South China Sea region. *Tectonophysics* 235, 149–180. doi:10.1016/0040-1951(94)90022-1

Lei, C., Ren, J., Pei, J., Liu, B., Zuo, X., Liu, J., et al. (2021). Tectonics of the offshore Red River Fault recorded in the junction of the yinggehai and Qiongdongnan basins. *Sci. China Earth Sci.* 64, 1893–1908. doi:10.1007/s11430-020-9796-2

Leloup, P. H., Lacassin, R., Tapponnier, P., Schärer, U., Zhong, D., Liu, X., et al. (1995). The Ailao Shan-Red River shear zone (yunnan, China), Tertiary transform boundary of Indochina. *Tectonophysics* 251, 3–84. doi:10.1016/0040-1951(95)00070-4

Li, C.-F., Xu, X., Lin, J., Sun, Z., Zhu, J., Yao, Y., et al. (2014). Ages and magnetic structures of the South China Sea constrained by deep tow magnetic surveys and IODP Expedition 349. *Geochem. Geophys. Geosyst.* 15, 4958–4983. doi:10.1002/2014GC005567

Li, G., Mei, L., Pang, X., Zheng, J., Ye, Q., and Hao, S. (2022). Magmatism within the northern margin of the South China Sea during the post-rift stage: An overview, and new insights into the geodynamics. *Earth-Science Rev.* 225, 103917. doi:10.1016/j.earscirev.2022.103917

Li, H., Chen, S., Zhang, Y., Niu, C., Zhang, K., Ye, Q., et al. (2014). Faults in the Zhu III depression of Pearl River Mouth basin and their control over hydrocarbon accumulation. *Mar. Geol. Quat. Geol.* 34, 115–124. doi:10.3724/SP.J.1140.2014.03115

Li, S., Suo, Y., Liu, X., Dai, L., Yu, S., Zhao, S., et al. (2012). Basin structural pattern and tectonic models of the South China sea: Problems, advances and controversies. *Mar. Geol. Quat. Geol.* 32, 35–53. doi:10.3724/SP.J.1140.2012.06035

Li, S., Suo, Y., Zhou, J., Wang, G., Li, X., Jiang, Z., et al. (2022). Tectonic evolution of the South China ocean-continent connection zone: Transition and mechanism of the Tethyan to the Pacific tectonic domains. *J. Geomechanics* 28. doi:10.12090/j.issn.1006-6616.20222809

Li, Y., Zhu, R., Liu, H., Qiu, X., and Huang, H. (2019). The cenozoic activities of yangjiang-yitongdong fault: Insights from analysis of the tectonic characteristics and evolution processes in Western Zhujiang (Pearl) River Mouth basin. *Acta Oceanol. Sin.* 38, 87–101. doi:10.1007/s13131-019-1477-x

Liang, H., Campbell, I. H., Allen, C. M., Sun, W., Yu, H., Xie, Y., et al. (2007). The Age of the Potassic Alkaline igneous rocks along the Ailao Shan–Red River shear zone: Implications for the onset Age of left-lateral shearing. *J. Geol.* 115, 231–242. doi:10.1086/510801

Liu, H., Mei, L., Shi, H., Shu, Y., Tian, W., and Ye, Q. (2018). Rift style controlled by basement attribute and regional stress in Zhu depression, Pearl River Mouth Basin. *Earth Sci.* 1–17. doi:10.3799/dqkx.2018.576

Liu, J., Chen, X., Wu, W., Tang, Y., Tran, M.-D., Nguyen, Q.-L., et al. (2015). New tectono-geochronological constraints on timing of shearing along the Ailao Shan-Red River shear zone: Implications for Genesis of Ailao Shan gold mineralization. *J. Asian Earth Sci.* 103, 70–86. doi:10.1016/j.jseaes.2014.11.006

Liu, J., Tang, Y., Tran, M.-D., Cao, S., Zhao, L., Zhang, Z., et al. (2012). The nature of the Ailao Shan–Red River (ASRR) shear zone: Constraints from structural, microstructural and fabric analyses of metamorphic rocks from the Diancang Shan, Ailao Shan and Day Nui Con Voi massifs. *J. Asian Earth Sci.* 47, 231–251. doi:10.1016/j.jseaes.2011.10.020

Liu, S., Gurnis, M., Ma, P., and Zhang, B. (2017). Reconstruction of northeast Asian deformation integrated with Western Pacific plate subduction since 200 Ma. *Earth-Science Rev.* 175, 114–142. doi:10.1016/j.earscirev.2017.10.012

Liu, X., Wu, J., Zhu, D., Suo, Y., Zhou, J., Wang, P., et al. (2021). Superimposition of strike-slip faults and pull-apart basins in the Pearl River Mouth basin: A case study from the eastern Yangjiang sag. *Geotect. Metallogenia* 45, 6–19. doi:10.16539/j.ddgzyckx.2021.01.002

Liu, Y., Wu, Z., Liu, L., Yan, S., Hu, L., Ping, M., et al. (2021). Cenozoic structure and tectonics of north subbasins in Beibu Gulf basin, northern south China sea. *Tectonophysics* 812, 228912. doi:10.1016/j.tecto.2021.228912

Liu, Z., Wang, S., Yin, B., Zhang, Y., and Xiao, L. (2013). Nephrology in China. *Nat. Rev. Nephrol.* 35, 523–528. doi:10.1038/nrneph.2013.146

Lu, B., Wang, P., Zhang, G., Zhang, B., Sun, X., Li, W., et al. (2011). Basement structures of an epicontinental basin in the northern South China Sea and their significance in petroleum prospect. *Acta Pet. Sin.* 32, 580–587. doi:10.1007/s12182-011-0123-3

Lv, C., Zhang, G., and Yang, D. (2017). Differential structure and dynamic mechanism of Wenchang Formation in the Zhu depression of the Pearl River Mouth basin. *Earth Sci. Front.* 24, 333–341. doi:10.13745/j.esf.yx.2016-11-56

Ma, B., Qi, J., Chen, W., and Zhao, M. (2020). Fault interaction and evolution during two-phase rifting in the Xijiang sag , Pearl River Mouth basin , northern south China sea. *Geol. J.* 55, 1128–1147. doi:10.1002/gj.3474

Ma, M., Liu, C., Qi, J., Zhang, D., Zhang, S., Wang, J., et al. (2020). Cenozoic subsidence history of the Pearl River Mouth basin, northern south China sea. *Geol. J.* 55, 750–770. doi:10.1002/gj.3439

Madon, M., Kim, C. L., and Wong, R. (2013). The structure and stratigraphy of deepwater Sarawak, Malaysia: Implications for tectonic evolution. *J. Asian Earth Sci.* 76, 312–333. doi:10.1016/j.jseaes.2013.04.040

Mcclay, K. (2001). Analog models of restraining stopovers in strike-slip fault systems. *AAPG Bull.* 85, 233–260. doi:10.1016/S0378-7753(00)00605-4

Mu, D., Peng, G., Zhu, D., Li, S., Suo, Y., Zhan, H., et al. (2022). Structure and formation mechanism of the Pearl River Mouth basin: Insights from multi-phase strike-slip motions in the Yangjiang sag, SE China. *J. Asian Earth Sci.* 226, 105081. doi:10.1016/j.jseaes.2022.105081

Müller, R. D., Sdrolias, M., Gaina, C., and Roest, W. R. (2008). Age, spreading rates, and spreading asymmetry of the world's ocean crust: Digital Models of the World's Ocean Crust. *Geochem. Geophys. Geosyst.* 9, Q04006. doi:10.1029/2007GC001743

Northrup, C. J., Royden, L. H., and Burchfiel, B. C. (1995). Motion of the Pacific plate relative to Eurasia and its potential relation to Cenozoic extension along the eastern margin of Eurasia. *Geol.* 23, 719. doi:10.1130/0091-7613(1995)023<0719:motppr>2.3.co;2

Ren, J. (2018). Genetic dynamics of China offshore Cenozoic basins. *Earth Sci.* 43, 3337–3361. doi:10.3799/dqkx.2018.330

Romeo, I., Capote, R., and Anguita, F. (2005). Tectonic and kinematic study of a strike-slip zone along the southern margin of Central Ovda Regio, Venus: Geodynamical implications for crustal plateaux formation and evolution. *Icarus* 175, 320–334. doi:10.1016/j.icarus.2004.11.007

Shen, M., Shan, X., Hao, G., Liu, P., Jia, P., Xu, C., et al. (2022). Structural difference and control mechanism of early Cenozoic depression in Yangjiang east sag, Pearl River Mouth Basin. *Earth Sci.*, 1–23. doi:10.3799/dqkx.2022.078

Shi, H., Du, J., Mei, L., Zhang, X., Hao, S., Liu, P., et al. (2020). Huizhou Movement and its significance in Pearl River Mouth Basin, China. *Pet. Explor. Dev.* 47, 483–498. doi:10.1016/S1876-3804(20)60067-2

Sibuet, J.-C., Yeh, Y.-C., and Lee, C.-S. (2016). Geodynamics of the South China sea. *Tectonophysics* 692, 98–119. doi:10.1016/j.tecto.2016.02.022

Sun, W. (2016). Initiation and evolution of the South China sea: An overview. *Acta Geochim.* 35, 215–225. doi:10.1007/s11631-016-0110-x

Sun, Z., Xu, Z., Sun, L., Pang, X., Yan, C., Li, Y., et al. (2014). The mechanism of post-rift fault activities in Baiyun sag, Pearl River Mouth basin. *J. Asian Earth Sci.* 89, 76–87. doi:10.1016/j.jseaes.2014.02.018

Sun, Z., Zhong, Z., Zhou, D., Pang, X., Huang, C., Chen, C., et al. (2008). Dynamics analysis of the Baiyun sag in the Pearl River Mouth basin, north of the South China sea. *Acta Geol. Sin.* 82, 73–83. doi:10.1111/j.1755-6724.2008.tb00326.x

Sun, Z., Zhou, D., Wu, S., Zhong, Z., Jiang, J., Fan, H., et al. (2009). Patterns and dynamics of rifting on passive continental margin from shelf to slope of the northern south China sea: Evidence from 3D analogue modeling. *J. Earth Sci.* 20, 136–146. doi:10.1007/s12583-009-0011-6

Sun, Z., Zhou, D., Zhong, Z., Zeng, Z., and Wu, S. (2003). Experimental evidence for the dynamics of the formation of the Yinggehai basin, NW South China Sea. *Tectonophysics* 372, 41–58. doi:10.1016/S0040-1951(03)00230-0

Suo, Y., Li, S., Peng, G., Du, X., Zhou, J., Wang, P., et al. (2022). Cenozoic basement-involved rifting of the northern South China Sea margin. *Gondwana Res.* doi:10.1016/j.gr.2022.02.017

Tang, X., Yang, S., and Hu, S. (2020). Provenance of the Paleogene sediments in the Pearl River Mouth basin, northern south China sea: Insights from zircon U-Pb and fission track double dating. *J. Asian Earth Sci.* 200, 104494. doi:10.1016/j.jseaes.2020.104494

Tang, Y., Liu, J., Tran, M.-D., Song, Z., Wu, W., Zhang, Z., et al. (2013). Timing of left-lateral shearing along the Ailao Shan-Red River shear zone: Constraints from zircon U–Pb ages from granitic rocks in the shear zone along the Ailao Shan Range, western yunnan, China. *Int. J. Earth Sci.* 102, 605–626. doi:10.1007/s00531-012-0831-y

Tapponnier, P., Lacassin, R., Leloup, P. H., Sch?Rer, U., Dalai, Z., Haiwei, W., et al. (1990). The Ailao Shan/Red River metamorphic belt: Tertiary left-lateral shear between Indochina and south China. *Nature* 343, 431–437. doi:10.1038/343431a0

Torsvik, T. H., Müller, R. D., Van der Voo, R., Steinberger, B., and Gaina, C. (2008). Global plate motion frames: Toward a unified model. *Rev. Geophys.* 46, RG3004. doi:10.1029/2007RG000227

Wang, H., Cao, S., Li, J., Cheng, X., Lv, M., Manfred, B., et al. (2019). Cenozoic multi-metamorphism, shear deformation and geological significance of Ailaoshan high-grade metamorphic complex, Western Yunnan, China. *Acta Petrol. Sin.* 35, 2573–2596. doi:10.18654/1000-0569/2019.08.15

Wang, J., Luan, X., He, B., Ran, W., Wei, X., Hu, Q., et al. (2021a). Study on the structural characteristics and dynamic mechanism of faults in the Kaiping sag of Zhujiang River Mouth basin. *Acta Oceanol. Sin.* 43, 41–53. doi:10.12284/hyxb2021082

Wang, J., Luan, X., He, B., Ran, W., Zhang, H., and Yang, J. (2021b). Characteristics and genesis of faults in southwestern Pearl River Mouth basin, northern south China sea. *Earth Sci.* 46, 916–928. doi:10.3799/dqkx.2020.381

Wang, J., Pang, X., Tang, D., Liu, B., and Xu, D. (2013). Transtensional tectonism and its effects on the distribution of sandbodies in the Paleogene Baiyun sag, Pearl River Mouth basin, China. *Mar. Geophys. Res.* 34, 195–207. doi:10.1007/s11001-013-9200-x

Wang, P., Li, S., Guo, L., Zhao, S., Li, X., Wang, Y., et al. (2017). Opening of the South China sea (SCS): A joint effect of dextral strike-slip pull-apart and proto-SCS slab pull. *Earth Sci. Front.* 24, 294–319. doi:10.13745/j.esf.yx.2017-4-3

Wang, P., Li, S., Suo, Y., Guo, L., Santosh, M., Li, X., et al. (2021). Structural and kinematic analysis of cenozoic rift basins in south China sea: A synthesis. *Earth-Science Rev.* 216, 103522. doi:10.1016/j.earscirev.2021.103522

Wang, P., Li, S., Suo, Y., Guo, L., Wang, G., Hui, G., et al. (2020). Plate tectonic control on the formation and tectonic migration of Cenozoic basins in northern margin of the South China Sea. *Geosci. Front.* 11, 1231–1251. doi:10.1016/j.gsf.2019.10.009

Wang, P., Suo, Y., Peng, G., Li, S., Du, X., Cao, X., et al. (2022). Three-stage extension in the cenozoic Pearl River Mouth basin triggering onset of the South China sea spreading. *Gondwana Res.* doi:10.1016/j.gr.2022.05.023

Wang, T. K., Chen, M.-K., Lee, C.-S., and Xia, K. (2006). Seismic imaging of the transitional crust across the northeastern margin of the South China Sea. *Tectonophysics* 412, 237–254. doi:10.1016/j.tecto.2005.10.039

Wang, W., Ye, J., Bidgoli, T., Yang, X., Shi, H., and Shu, Y. (2017). Using Detrital zircon Geochronology to constrain Paleogene provenance and its relationship to rifting in the Zhu 1 depression, Pearl River Mouth basin, south China sea. *Geochem. Geophys. Geosyst.* 18, 3976–3999. doi:10.1002/2017GC007110

Wang, W., Zhou, W., Shan, X., and Liu, Y. (2015). Characteristics of hidden fault zone and its significance in geology in sedimentary basin. *J. Central South Univ.* 46, 2236–2243. doi:10.11817/j.issn.1672-7207.2015.06.035

Wang, X., Yu, S., Gong, Y., Li, S., Liu, X., Ma, Y., et al. (2014). Extension of NE-trending faults in south China to northern south China sea continental shelf. *Geotect. Metallogenia* 38, 557–570. doi:10.16539/j.ddgzyckx.2014.03.005

Wei, X., Ruan, A., Zhao, M., Qiu, X., Li, J., Zhu, J., et al. (2011). A wide-angle obs profile across the Dongsha uplift and chaoshan depression in the mid-northern South China sea. China. *J. Geophys.* 54, 3325–3335. doi:10.3969/j.issn.0001-5733.2011.12.030

Wu, S., Gao, J., Zhao, S., Lüdmann, T., Chen, D., and Spence, G. (2014). Post-rift uplift and focused fluid flow in the passive margin of northern South China Sea. *Tectonophysics* 615–616, 27–39. doi:10.1016/j.tecto.2013.12.013

Xie, H., Zhou, D., Li, Y., Pang, X., Li, P., Chen, G., et al. (2014). Cenozoic tectonic subsidence in deepwater sags in the Pearl River Mouth basin, northern south China sea. *Tectonophysics* 615–616, 182–198. doi:10.1016/j.tecto.2014.01.010

Xu, J., Ben-Avraham, Z., Kelty, T., and Yu, H.-S. (2014). Origin of marginal basins of the NW Pacific and their plate tectonic reconstructions. *Earth-Science Rev.* 130, 154–196. doi:10.1016/j.earscirev.2013.10.002

Xu, J., and Zhang, L. (2000). Genesis of cenozoic basins in northwest Pacific margin (2): Linked dextral pull apart basin system. *Oil Gas Geol.* 03, 185–190. doi:10.3321/j.issn:0253-9985.2000.03.001

Yan, Q., Shi, X., Yuan, L., Yan, S., and Liu, Z. (2022). Tectono-magmatic evolution of the Philippine sea plate: A review. *Geosystems Geoenvironment* 1, 100018. doi:10.1016/j.geogeo.2021.100018

Ye, Q., Mei, L., Shi, H., Du, J., Deng, P., Shu, Y., et al. (2020). The influence of pre-existing basement faults on the cenozoic structure and evolution of the proximal domain, northern south China sea rifted margin. *Tectonics* 39. doi:10.1029/2019TC005845

Ye, Q., Mei, L., Shi, H., Shu, Y., Camanni, G., and Wu, J. (2018). A low-angle normal fault and basement structures within the Enping sag, Pearl River Mouth basin: Insights into late Mesozoic to early cenozoic tectonic evolution of the South China sea area. *Tectonophysics* 731, 1–16. doi:10.1016/j.tecto.2018.03.003

Yu, C., Han, Q., Dong, D., Chen, S., and Yan, P. (2008). Estimation of cenozoic dextral strike-slip displacement of tan-Lu fault in laizhou Bay. *Nat. Gas. Geosci.* 19, 62–69. doi:10.11764/j.issn.1672-1926.2008.01.62

Yu, Y., Zhang, T., Zhang, Z., Zhang, G., Zeng, J., Yang, H., et al. (2021). Structural characteristics and its Significances on hydrocarbon accumulation in the Yunkai low uplift, Pearl River Mouth basin. *Acta Geol. sinica-. Engl. Ed.* 95, 21–29. doi:10.1111/1755-6724.14622

Zhan, H., Cai, G., Zhang, Z., Wang, G., Li, Y., Suo, Y., et al. (2021). Paleogene Fault activity and basin controlling characteristics in the northern south China sea margin—a case study of the eastern Yangjiang sag. *Geotect. Metallogenia* 45, 20–39. doi:10.16539/j.ddgzyckx.2021.01.003

Zhang, C., Wang, Z., Sun, Z., Sun, Z., Liu, J., and Wang, Z. (2013). Structural differences between the Western and eastern Qiongdongnan basin: Evidence of Indochina block extrusion and south China sea seafloor spreading. *Mar. Geophys. Res.* 34, 309–323. doi:10.1007/s11001-013-9187-3

Zhang, G., Qu, H., Jia, Q., Zhang, L., Yang, B., Chen, S., et al. (2021). Passive continental margin segmentation of the marginal seas and its effect on hydrocarbon accumulation: A case study of the northern continental margin in south China sea. *Mar. Petroleum Geol.* 123, 104741. doi:10.1016/j.marpetgeo.2020.104741

Zhang, Y., Qi, J., and Wu, J. (2019). Cenozoic faults systems and its geodynamics of the continental margin basins in the northern of South China Sea. *Earth Sci.* 44, 603–625. doi:10.3799/dqkx.2018.542

Zhao, F., Alves, T. M., Xia, S., Li, W., Wang, L., Mi, L., et al. (2020). Along-strike segmentation of the South China Sea margin imposed by inherited pre-rift basement structures. *Earth Planet. Sci. Lett.* 530, 115862. doi:10.1016/j.epsl.2019.115862

Zhao, Y., Ren, J., Pang, X., Yang, L., and Zheng, J. (2018). Structural style, formation of low angle normal fault and its controls on the evolution of Baiyun Rift, northern margin of the South China Sea. *Mar. Petroleum Geol.* 89, 687–700. doi:10.1016/j.marpetgeo.2017.11.001

Zhao, Z., Sun, Z., Sun, L., Wang, Z., and Sun, Z. (2018). Cenozoic tectonic subsidence in the Qiongdongnan basin, northern south China sea. *Basin Res.* 30, 269–288. doi:10.1111/bre.12220

Zhong, Z., Shi, H., Zhu, M., Pang, X., He, M., Zhao, Z., et al. (2014). A discussion on the tectonic-stratigraphic framework and its origin mechanism in Pearl River Mouth Basin. *China Offshore Oil Gas* 26, 20–29.

Zhou, J., Li, S., Suo, Y., Zhang, L., Du, X., Cao, X., et al. (2022). NE-Trending transtensional faulting in the Pearl River Mouth basin of the northern south China sea margin. *Gondwana Res.* doi:10.1016/j.gr.2022.02.016

Zhou, D., Wang, W., Wang, J., Pang, X., Cai, D., and Sun, Z. (2006). Mesozoic subduction-accretion zone in northeastern south China Sea inferred from geophysical interpretations. *Sci. China Ser. D* 49, 471–482. doi:10.1007/s11430-006-0471-9

Zhou, W., Zhuo, H., Wang, Y., Xu, Q., and Li, D. (2020). Post-rift submarine volcanic complexes and fault activities in the Baiyun sag, Pearl River Mouth basin: New insights into the breakup sequence of the northern south China sea. *Mar. Geol.* 430, 106338. doi:10.1016/j.margeo.2020.106338

Zhou, Z., Mei, L., Liu, J., Zheng, J., Chen, L., and Hao, S. (2018). Continentward-dipping detachment fault system and asymmetric rift structure of the Baiyun Sag, northern South China Sea. *Tectonophysics* 726, 121–136. doi:10.1016/j.tecto.2018.02.002

Zhou, Z., Mei, L., Shi, H., and Shu, Y. (2019). Evolution of low-angle normal faults in the Enping sag, the northern south China sea: Lateral growth and vertical rotation. *J. Earth Sci.* 30, 1326–1340. doi:10.1007/s12583-019-0899-4

Zhu, M., Graham, S., and McHargue, T. (2009). The Red River Fault zone in the yinggehai basin, south China sea. *Tectonophysics* 476, 397–417. doi:10.1016/j.tecto.2009.06.015

Zhu, W., Huang, B., Mi, L., Wilkins, R. W. T., Fu, N., and Xiao, X. (2009). Geochemistry, origin, and deep-water exploration potential of natural gases in the Pearl River Mouth and Qiongdongnan basins, South China Sea. *Bulletin* 93, 741–761. doi:10.1306/02170908099

Zhu, W., Shi, H., Huang, B., Zhong, K., and Huang, Y. (2021). Geology and geochemistry of large gas fields in the deepwater areas, continental margin basins of northern South China Sea. *Mar. Petroleum Geol.* 126, 104901. doi:10.1016/j.marpetgeo.2021.104901

Zhu, W., Xie, X., Wang, Z., Zhang, D., Zhang, C., Cao, L., et al. (2017). New insights on the origin of the basement of the Xisha uplift, south China sea. *Sci. China Earth Sci.* 60, 2214–2222. doi:10.1007/s11430-017-9089-9